UNIVERSIDADE ESTADUAL PAULISTA
"JÚLIO DE MESQUITA FILHO"
Câmpus de São José do Rio Preto

Gustavo Sanghikian Marques dos Santos

Co_3O_4-ZnO heterostructure for microbial volatile organic compounds detection

São José do Rio Preto
2023

Gustavo Sanghikian Marques dos Santos

Co_3O_4-ZnO heterostructure for microbial volatile organic compounds detection

Dissertation presented as part of the requirements for obtaining the Master's degree in Chemistry at the Program of Postgraduation in Chemistry at the Institute of Biosciences, Letters and Exact Sciences of the Universidade Estadual Paulista "Júlio de Mesquita Filho," Campus of São José do Rio Preto.
Financier: CAPES

Advisor: Prof. Dr. Diogo Paschoalini Volanti

São José do Rio Preto
2023

S237c

Santos, Gustavo Sanghikian Marques dos
Co3O4-ZnO heterostructure for microbial volatile organic compounds detection / Gustavo Sanghikian Marques dos Santos. -- São José do Rio Preto, 2023
35 p. : il., tabs., fotos

Dissertação (mestrado) - Universidade Estadual Paulista (Unesp), Instituto de Biociências Letras e Ciências Exatas, São José do Rio Preto
Orientador: Diogo Paschoalini Volanti

1. Semiconductors. 2. Sensor. 3. Microbial volatile organic compounds. 4. Metal-organic framework. 5. Heterostructure. I. Título.

Sistema de geração automática de fichas catalográficas da Unesp. Biblioteca do Instituto de Biociências Letras e Ciências Exatas, São José do Rio Preto. Dados fornecidos pelo autor(a).

Essa ficha não pode ser modificada.

IMPACTO SOCIAL DA DISSERTAÇÃO

O impacto social deste trabalho está relacionado com a detecção dos compostos orgânicos voláteis microbianos produzidos por microorganismos, possibilitando uma melhor compreensão sobre seus efeitos. Além disso, é um material sintetizado através de um processo não tóxico e sustentável.

DISSERTATION SOCIAL IMPACT

The social impact of this work is related to the detection of microbial volatile organic compounds produced by microorganisms, enabling a better understanding of their effects. Furthermore, it is a material synthesized through a non-toxic and sustainable process.

Gustavo Sanghikian Marques dos Santos

Co_3O_4-ZnO heterostructure for microbial volatile organic compounds detection

Dissertation presented as part of the requirements for obtaining the Master's degree in Chemistry at the Program of Postgraduation in Chemistry at the Institute of Biosciences, Letters and Exact Sciences of the Universidade Estadual Paulista "Júlio de Mesquita Filho," Campus of São José do Rio Preto.
Financier: CAPES

Advisor: Prof. Dr. Diogo Paschoalini Volanti

Examining Committee

Prof. Dr. Diogo Paschoalini Volanti
UNESP – Câmpus de São José do Rio Preto
Orientador

Prof. Dr. Thiago Augusto de Lima Burgo
UNESP – Câmpus de São José do Rio Preto

Drª. Talita Mazon
Centro de Tecnologia da Informação – Campinas/SP

São José do Rio Preto
October 9th, 2023

ACKNOWLEDGEMENTS

I would first like to thank my family, especially my parents, Wiris and Ana Paula, for the love and support they always gave me. I also thank my advisor, Professor Diogo, for providing all the structure and support for my academic education. I am grateful to my friends, especially Bruna Sá, for the partnership and fundamental teachings for my growth. Thanks to the LSQA/IBILCE-UNESP laboratories for providing the XRD and FTIR techniques, to the LMA/IQ-UNESP for the FESEM and EDX and the LNLS-SIRIUS for the XPS and XAS.

This work was carried out with the support of the Coordination for the Improvement of Higher Education Personnel - Brazil (CAPES) - Financing Code 001.

RESUMO

O foco desse trabalho foi sintetizar heteroestruturas *p-n* e *n-p* à base de Co_3O_4-ZnO e ZnO-Co_3O_4, derivados de estruturas metal-orgânicas (metal-organic frameworks, MOF) para detectar moléculas voláteis produzidas por micro-organismos (ex.: fungos e bactérias). Entretanto, existem poucos estudos na detecção rápida e com limite de detecção baixo de compostos orgânicos voláteis produzidos por micro-organismos (microbial volatile organic compounds, MVOCs). O estudo foi composto pela avaliação do uso de heteroestruturas *p-n* e *n-p* em comparação com a estrutura pura do óxido de cobalto (Co_3O_4) para aprimorar a resposta, a seletividade e o tempo de resposta na detecção de MVOCs, principalmente para o 3-metil-1-butanol. Os sensores foram preparados a partir da degradação térmica em atmosfera comum das MOFs (ZIF-8/ZIF-67) preparadas previamente por um método hidrotérmico simples, utilizando dos sais $Co(NO_3)_2.6H_2O$ e $Zn(NO_3)_2.6H_2O$ e o ligante orgânico 2-metilimidazol em água deionizada. Os resultados de caracterização desses materiais demonstraram que as amostras não apresentaram impurezas ou surgimento de fases indesejadas. As respostas dos sensores foram avaliadas na faixa de 100 partes por milhão (100 ppm) dos MVOCs: 2-nonanona, etanol, 3-metil-1-butanol, acetona e acetato de etila, variando a temperatura de operação na faixa de 190-350 °C. A maior resposta de 14,6 foi para o 3-metil-1-butanol demonstrado pelo sensor heteroestruturado Co_3O_4-ZnO na temperatura ótima de 270 °C. Além disso, esse sensor apresentou um bom desempenho na detecteção do 3-metil-1-butanol com a presença de atmosfera úmida em diferentes faixas de umidade relativa controlada. Por fim, foi possível observar uma melhora significativa nas propriedades sensoras da heteroestrura *p-n* Co_3O_4-ZnO em comparação ao óxido puro de Co_3O_4.

Palavras-chave da dissertação: Semicondutores. Sensor de gás. Heteroestrutura *p-n*. Óxido de cobalto. Óxido de zinco. 3-metil-1-butanol.

ABSTRACT

This work focused on synthesizing *p-n* and *n-p* heterostructures based on Co_3O_4-ZnO and ZnO-Co_3O_4, derived from metal-organic frameworks (MOF) to detect volatile molecules produced by microorganisms (fungi and bacteria). However, there are few studies on the rapid detection and low detection limit of volatile organic compounds produced by microorganisms (microbial volatile organic compounds, MVOCs). The study consisted of evaluating the use of *p-n* and *n-p* heterostructures in comparison with the pure structure of cobalt oxide (Co_3O_4) to improve the response, selectivity, and response time in the detection of MVOCs, mainly for 3-methyl- 1-butanol. The sensors were prepared from thermal degradation in a typical atmosphere of MOFs (ZIF-8/ZIF-67) previously prepared by a simple hydrothermal method, using the salts $Co(NO_3)_2.6H_2O$ and $Zn(NO_3)_2.6H_2O$ and the organic ligand 2-methylimidazole in deionized water. The characterization results of these materials demonstrated that the samples did not present impurities or the appearance of unwanted phases. Sensor responses were evaluated in the range of 100 parts per million (100 ppm) of the MVOCs: 2-nonanone, ethanol, 3-methyl-1-butanol, acetone, and ethyl acetate, varying the operating temperature in the range of 190- 350 °C. The highest response of 14.6 was for 3-methyl-1-butanol, demonstrated by the Co_3O_4-ZnO heterostructured sensor at the optimum temperature of 270 °C. Furthermore, this sensor performed well in detecting 3-methyl-1-butanol in a humid atmosphere in different ranges of controlled relative humidity. Finally, it was possible to observe a significant improvement in the sensing properties of the Co_3O_4-ZnO *p-n* heterostructure compared to pure Co_3O_4 oxide.

Dissertation Keywords: Semiconductors. Gas sensor. *P-n* heterostructure. Cobalt oxide. Zinc oxide,. 3-methyl-1-butanol.

ABBREVIATIONS AND ACRONYMS LIST

2-MI	2-methylimidazole
3M1B	3-methyl-1-butanol
BET	Brunauer-Emmett-Teller
DI	Deionized
EDX	Energy-dispersive X-ray
FESEM	Field emission scanning electron microscopy
FTIR	Fourier transform infrared spectroscopy
MOF	Metal-organic framework
MVOC	Microbial volatile organic compound
RH	Relative humidity
SMO	Semiconducting metal oxide
TEY	Total electron-yield
TFY	Total fluorescence-yield
XAS	X-ray absorption spectroscopy
XPS	X-ray photoelectron spectroscopy
XRD	X-ray diffraction
ZIF	Zeolitic imidazole framework

SYMBOLS LIST

Å	Ångström
°C	Celsius degree
cm	Centimeter
cm^3/g	Cubic centimetre per gram
eV	Electron volt
g	Gram
h	Hour
keV	Kilo electron volt
kV	Kilovolt
mA	Milliampère
mg	Milligram
mL	Milliliter
mmol	Millimol
min	Minute
ppm	Parts per million
s	Second
$m^2\ g^{-1}$	Square meter per gram

SUMMARY

CHAPTER 1: General introduction and aim of this dissertation.

Over the years, problems related to human health have become a big concern in society. Among these problems, the presence of micro-organisms in the spoilage process of food and diseases in people caused by these pathogens are relevant discussions (THORN; GREENMAN, 2012). In this way, this present study sought to synthesize a material capable of assisting in the presence of fungi and bacteria detection. The micro-organisms produce microbial volatile organic compounds (MVOCs) during metabolism, with different organic compositions (POVEDA, 2021). Semiconductor oxides (SMOs) are materials suitable to apply as gas and MVOC sensors, such as Co_3O_4 (XU; CHENG, 2016) and ZnO (ZHANG et al., 2019). However, the pure oxides as sensors generally present low responses and poor selectivity. The *p-n* heterojunction is an excellent alternative to improve these sensing properties (LIU et al., 2022). So, MVOC detection using SMOs is a crucial way to improve health conditions and bring a database of these compounds.

The main objective of this study is to improve the pure Co_3O_4 sensing performance as an MVOC sensor with a *p-n* heterojunction of Co_3O_4-ZnO or the *n-p* heterostructure of ZnO-Co_3O_4, using the MOF-derived synthesis method. For the secondary objectives: (a) study the influence of the *n-p* and *p-n* heterojunction of ZnO and Co_3O_4 for MVOC detection; (b) application of an MVOC sensor in different operation conditions, such as varying the relative humidity (R.H.) and temperature in the working atmosphere; (c) the synthesis of a material capable of detecting MVOCs at low concentrations (ppm) with high selectivity, fast response time, stability, and reversibility.

For a better understanding of the structure of this study, it is divided into four chapters. Chapter 1 is the present one, with a general discussion and the principal objectives of this work. Subsequently, Chapter 2 presents the bibliography review and the references used. Chapter 3 is the article content to be published in a sensor journal, containing all the materials and methods used and the results produced in the laboratory. Finally, Chapter 4 exhibits the dissertation conclusions, challenges to overcome, and future studies.

REFERENCES

LIU, H. et al. Construction of hollow NiO/ZnO p-n heterostructure for ultrahigh performance toluene gas sensor. **Materials Science in Semiconductor Processing**, v. 141, 1 abr. 2022.

POVEDA, J. **Beneficial effects of microbial volatile organic compounds (MVOCs) in plants**. **Applied Soil Ecology**Elsevier B.V., , 1 dez. 2021.

THORN, R. M. S.; GREENMAN, J. **Microbial volatile compounds in health and disease conditions**. **Journal of Breath Research**, jun. 2012.

XU, J. M.; CHENG, J. P. **The advances of Co3O4as gas sensing materials: A review**. **Journal of Alloys and Compounds**Elsevier Ltd, , 2016.

ZHANG, X. et al. ZIF-8 derived hierarchical hollow ZnO nanocages with quantum dots for sensitive ethanol gas detection. **Sensors and Actuators, B: Chemical**, v. 289, p. 144–152, 15 jun. 2019.

CHAPTER 2: Bibliographic review

2.1 Microbial volatile organic compounds (MVOCs)

The microbial volatile organic compounds (MVOCs) are essentially composed of products with a boiling point below 250 °C at atmospheric pressure and produced by microorganisms. Human exposure to MVOCs causes social and health problems worldwide, such as damage to the respiratory system, skin irritations, oral diseases, and other infections (THORN; GREENMAN, 2012). The presence of MVOCs in urban and agricultural environments is a reality nowadays, with the sizeable inappropriate use of resources and unnecessary waste. Furthermore, food contamination is also related to the MVOC's existence in the deterioration process, causing more diseases and is a big concern worldwide for healthcare conditions (WANG et al., 2016). In other words, exposure to these compounds is frequent, becoming a chronic problem.

The MVOCs are formed during fungi and bacteria's primary and secondary metabolism, especially in DNA synthesis and glucose metabolic oxidation (KORPI; JÄRNBERG; PASANEN, 2009). These compounds can be formed by different function groups, such as aromatic compounds, alcohols, sulfur compounds, esters, and fatty acids (WEISSKOPF; SCHULZ; GARBEVA, 2021). Moreover, each microorganism produces specific MVOCs, as shown in the examples in Fig. 1. The 3-methyl-1-butanol ($C_5H_{12}O$) is a primary alcohol, colorless, with a strong odor and is also an MVOC, which can be emitted by the *Pseudomonas spp.* in the spoilage of shrimp (FAN; SCHNEIDER; SARNOSKI, 2022a). Besides, the 3-methyl-1-butanol is also a quality indicator of seafood by the presence of *Salmonella Thyphimurium* in the spoilage process (KHOT; PANIGRAHI; LIN, 2011).

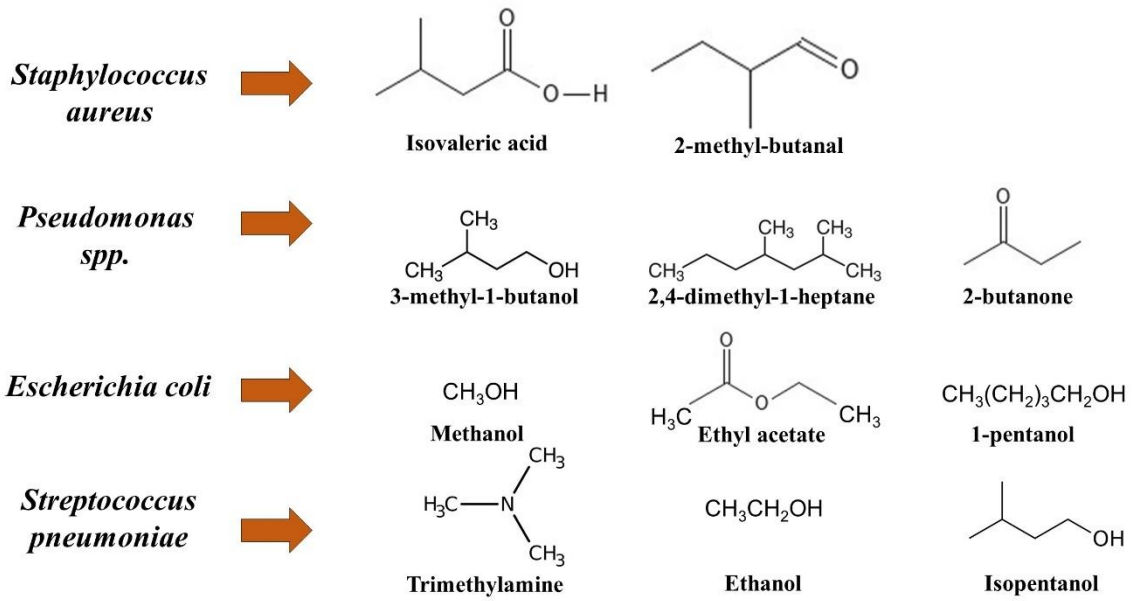

Fig. 1. Scheme of emission of MVOCs by different fungi and bacteria. Source: adapted from literature (BOS; STERK; SCHULTZ, 2013; FAN; SCHNEIDER; SARNOSKI, 2022b).

2.2 Semiconductors metal oxides based on ZnO and Co_3O_4 for MVOC detection

Semiconductors metal oxides (SMOs) are widely used for different applications, such as energetic components and batteries (SANTOS-CARBALLAL et al., 2023), solar cells (KISHORE KUMAR et al., 2020), photocatalysis (DJURIŠIĆ; LEUNG; CHING NG, 2014), supercapacitors (XU; LIU; LIU, 2016), and gas sensors (KRISHNA et al., 2022). In this way, an example of SMO is the wurtzite hexagonal structure of ZnO with a C_{6v} spatial group and a high band gap value of 3.37 eV (ARAÚJO et al., 2017). It is also an *n*-type semiconductor with significant use as a gas sensor due to its good properties, such as fast responses in gas sensing, excellent chemical stability, and no toxicity (WANG et al., 2020). Furthermore, the zinc metal comprises the 3*d* orbital filled with electrons. The *n*-type SMOs as gas sensors have oxygen vacancies in their composition, acting as electron donors during reactions with oxygen adsorbed on their surface (ZAKI et al., 2019). However, the *p*-type materials are barely used as gas sensors compared to the *n*-type ones (KIM; LEE, 2014). The Co_3O_4 presents a spinel structure and low band gap, with tetrahedral (T_d) Co^{2+} and octahedral (O_h) Co^{3+} ions, containing electronic configurations [Ar] $3d^7$ and [Ar] $3d^6$, respectively. Moreover, is a *p*-type semiconductor based on holes in the valence level and reacting with the oxygen adsorbed during the contact with the gas, releasing electrons (TURGUT et al., 2018). These mechanisms are based on the electronic transference caused by the reaction between the adsorbed oxygen and the contact with reducing gases, such as MVOCs.

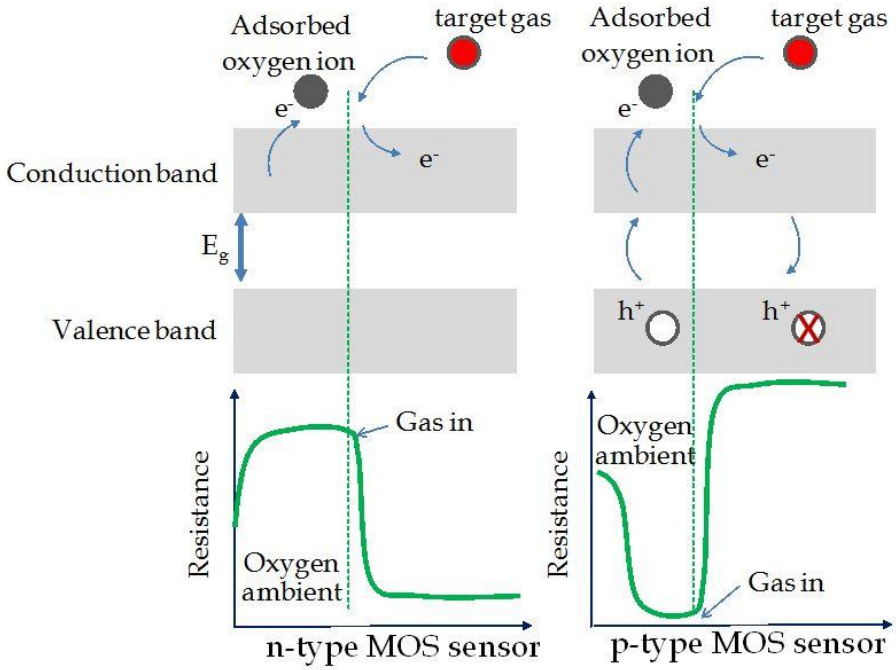

Fig. 2. Sensing mechanisms for *n*-type and *p*-type SMOs. Source: Choopun *et al.* 2012 (CHOOPUN; HONGSITH; WONGRAT, 2012).

The operating temperature for MVOC detection is crucial to the sensing process. This fact can be explained by how the sensor mechanism works during the reactions with the oxygen in contact with MVOCs. Different oxygen species are adsorbed and ionized on the surface of these materials. This mechanism is related to the sensor measurements, varying the selectivity and response values at their specific working temperature. In this way, O_2^- is the predominant oxygen species in the temperature range of 150 and 200 °C. The O^- and O^{2-} are formed at 200 to 400 °C. Above 400 °C, only the O^{2-} is mainly present (KIM; ROTHSCHILD; TULLER, 2013).

These electronic transitions cause differences in the resistance values of the SMOs, which are responsible for the response measurements, as shown in Fig. 2. In the *n*-type sensors, when in contact with reducing MVOCs, the oxygen species adsorbed in the material's surface are consumed, forming CO_2 and H_2O, releasing electrons to the conducting region, and decreasing the material's resistance. The response for MVOC detection is calculated based on this resistance change. As for the p-type sensors, the response is calculated by the increase in the material's resistance when in contact with reducing MVOC and reacting with the adsorbed oxygen. The released electron causes a decrease in the holes and the electrical conductivity, generating a high resistance value (MOKOENA; SWART; MOTAUNG, 2019).

2.3 Sensors based on the *p-n* heterojunction of SMOs

The improvements in sensing properties are crucial to SMOs achieving high performances as MVOC sensors. These properties are related to the capacity of the sensor to detect MVOCs with good selectivity, fast response time, sensibility, and stability. Moreover, lower operation temperatures are also an essential goal for MVOC detection, saving energy usage. Most pure SMOs present low performance and high operation temperatures as MVOC sensors, such as the *p*-type Co_3O_4. Thus, the p-n heterojunction between Co_3O_4 and ZnO is a potential system to overcome these negative factors. The *p-n* heterostructure comprises a main phase of *p*-type material modified with an *n*-type semiconductor, such as the Co_3O_4-ZnO. As for the *n-p* heterojunction, the ZnO-Co_3O_4 is an example of this *n*-type modification with a *p*-type addition.

Heterostructures generally present high sensing performances due to the easy adsorption of oxygen species and the electron depletion layer appearance, increasing the MVOC detection. As shown in Fig. 3, the heterojunction causes a transference of the electrons in a high to a low energy level, generating a Fermi energy equalization. Then, the heterostructure forms a stable depletion layer at the material's surface, upgrading the sensing properties with this combination of two SMOs (GAI et al., 2022).

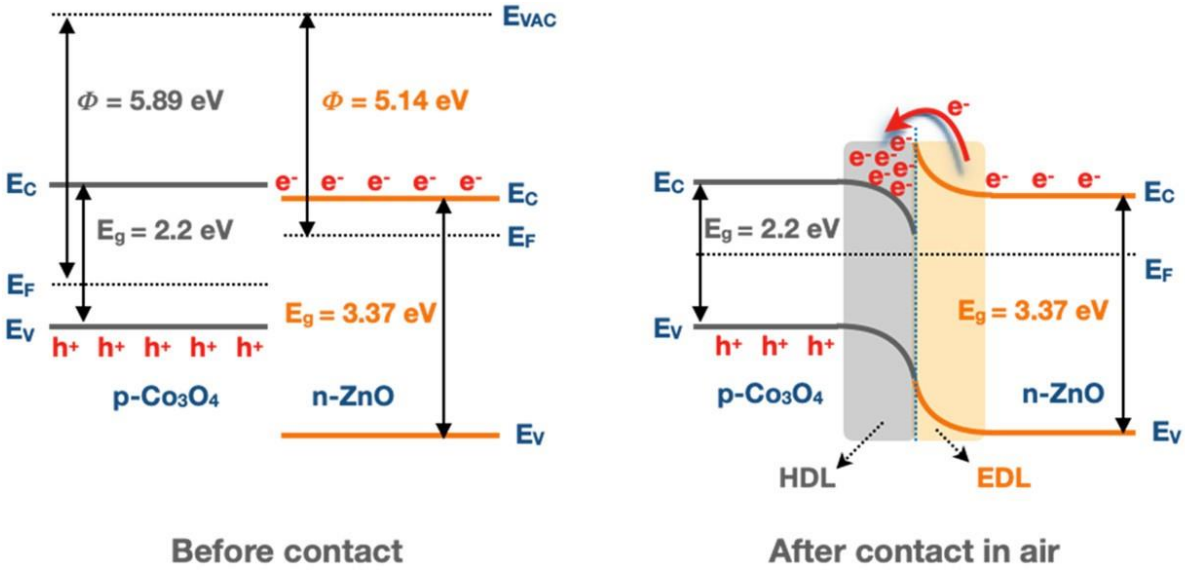

Fig. 3. Fermi energy equalization diagrams in the *p-n* heterojunction (a) before and (b) after contact in air. Source: adapted from Yan *et al*. 2021 (YAN et al., 2021).

The sensors based on heterojunctions are widely used for gas detection. As mentioned above, the easy oxygen adsorption and the formation of a stable depletion layer increase the sensing properties. In this way, Fig. 4 shows the sensor mechanism of a *p-n* heterostructure for formaldehyde gas detection composed of NiO and SnO_2. This example is similar to the present

study, exhibiting the formaldehyde detection process at the material's surface in a pure SnO_2 and a heterostructured material NiO/SnO_2 (Fig. 4a). The NiO presence increases the active sites for oxygen adsorption and, consequently, the formaldehyde sensing performance. These electronic changes exhibited by the NiO/SnO_2 are summarized in the band diagram, as shown in Fig. 4b.

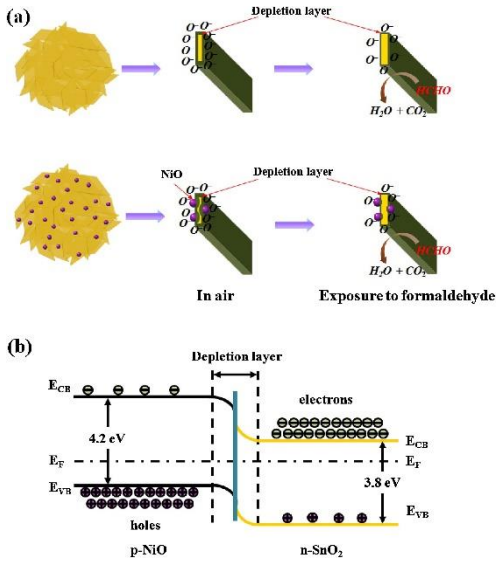

Fig. 4. (a) Sensing mechanism of formaldehyde detection using a *p-n* heterojunction. (b) Energy band diagram for NiO/SnO_2. Source: Meng *et al.* 2018 (MENG et al., 2018).

2.4 Metal-organic framework-derived SMO synthesis method

The metal-organic frameworks (MOFs) comprise hybrid crystalline materials formed with nodes containing metals interconnected by organic ligands. In this way, the MOFs present a porous network of up to three dimensions. Several types of MOFs, with a combination of metals and organic ligands, produce various materials with different morphologies. Besides, MOFs were already used for various applications, such as heterogeneous catalysis (LI; ARANISHI; XU, 2012), supercapacitors (YAN et al., 2016), drug liberation (SHU et al., 2017), and gas sensors (LÜ et al., 2014).

The MOF precursor synthesis for producing materials is a favorable process to obtain gas sensors. This affirmation is explained by the porosity, high specific surface area, and active sites presented by the MOFs, increasing the gas detection. Furthermore, these material's pore size and morphology increment the sensibility in the sensing process (YUAN et al., 2022). As for the MOF-derived SMOs for MVOC detection, these sensors can be obtained by the calcination process of the MOFs, maintaining the morphology and the porous structure. This thermal treatment must be controlled by choosing the temperature and heating rate to form the expected product, with the pore size distribution, surface area, and composition.

As discussed before, there are different examples of MOFs using a metal and organic ligand. The zeolitic imidazolate frameworks, such as ZIF-8 and ZIF-67, are examples of MOF precursors that can be applied to synthesize SMOs (ZnO and Co_3O_4, respectively). The ZIF-8 and ZIF-67 can be formed by reacting the 2-methylimidazole ($C_4H_6N_2$) and their respective metal in an inorganic salt form, using a solvent in a simple synthesis process, as shown in Fig. 5. Then, a three-dimensional structure, large pore size, and high specific surface area is obtained, already reported to be a great precursor for gas sensing (BAHOS et al., 2019).

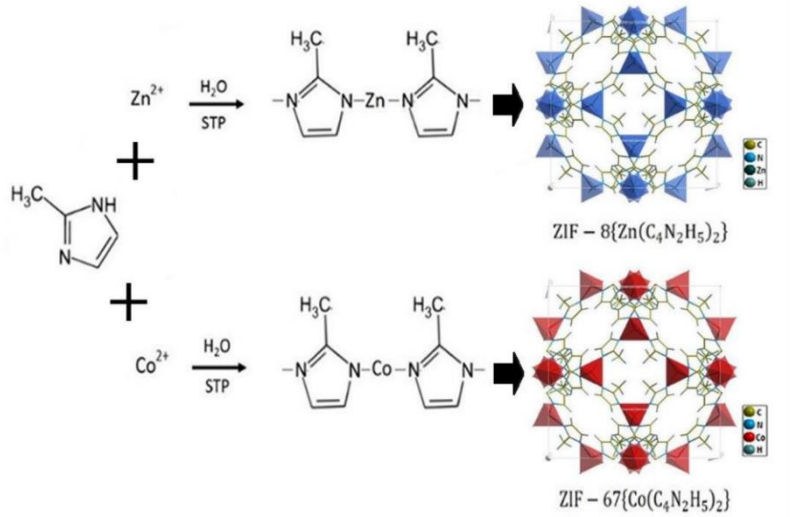

Fig. 5. Formation of the MOFs ZIF-8 and ZIF-67, composed of Zn^{2+} and Co^{2+}, respectively. Source: adapted from Bahos *et al*. 2019 (BAHOS et al., 2019).

CHAPTER 3: MOF-derived Co_3O_4-ZnO heterostructure for 3-methyl-1-butanol detection

Gustavo S. M. Santos[a], Bruna S. de Sá[a,b], Tarcísio M. Perfecto[c], Diogo P. Volanti*[a]

[a]*Laboratory of Materials for Sustainability (LabMatSus), São Paulo State University (UNESP), Rua Cristóvão Colombo 2265, 15054-000 São José do Rio Preto, Brazil*

[b]*Brazilian Agricultural Research Corporation (EMBRAPA), São Carlos, SP, 13560-970, Brazil*

[c]*Brazilian Nanotechnology National Laboratory, Brazilian Center for Research in Energy and Materials (CNPEM), Campinas, SP, 13083-970, Brazil*

**Corresponding author. E-mail address: diogo.volanti@unesp.br (Diogo P. Volanti)*

ABSTRACT

Microbial volatile organic compounds (MVOCs) detection with a fast response and high selectivity is barely studied. The challenge is developing a material that matches these factors in different sensing conditions, such as operating temperature and humidity. In this study, we searched for a better way to improve the gas sensing properties of cobalt oxide (Co_3O_4), synthesizing a MOF-derived (ZIF-67-ZIF-8) *p-n* heterojunction of Co_3O_4-ZnO, and varying the molar concentrations of these metals. The Co_3O_4 was synthesized by a mixture of cobalt(II) nitrate hexahydrate and 2-methylimidazole in a hydrothermal process, forming the ZIF-67 and then calcinating this material. The Co_3O_4-ZnO and ZnO-Co_3O_4 heterostructures were synthesized by adding zinc(II) nitrate hexahydrate to produce the ZIF-8 and make a heterojunction with ZIF-67, followed by calcination. The Co_3O_4-ZnO sample exhibited a higher sensing performance than the pure Co_3O_4 and the heterostructure ZnO-Co_3O_4. In this case, the Co_3O_4-ZnO showed a higher response of 14.6 to 3-methyl-1-butanol (3M1B) with a selectivity ratio of 2.79. Furthermore, this sensor demonstrated a response of 10.4 under 65% of relative humidity. So, improving the performance as a gas sensor of pure Co_3O_4 was possible with a *p-n* heterojunction of zinc and cobalt, indicating a suitable response under different conditions.

Keywords: gas sensor, semiconductor, metal-organic framework, cobalt oxide, 3-methyl-1-butanol.

3.1 Introduction

The metabolism of fungi and bacteria produces microbial volatile organic compounds (MVOCs), consisting of different chemical classes (hydrocarbons, alcohols, aromatic compounds, nitrogen, and sulfur-containing compounds) which are liberated by each microorganism [1–3]. Exposure to MVOCs causes different health and social problems worldwide, such as contamination of food [4] and human diseases [5–7]. An example of MVOC is the 3-methyl-1-butanol (3M1B), which can be produced by *Pseudomonas spp*. in the spoilage process of shrimp [8]. Furthermore, vapor can irritate the eyes [9], and a concentration of 3M1B is frequently presented at sugar factories in the waste of secondary products [10]. Although, studies are rarely reported in the literature on 3M1B detection [10,11]. Sensors of MVOCs with high selectivity and low cost are essential to improve healthcare conditions (food quality, healthful environments, and differentiating viral to bacterial diseases with accurate diagnoses, reducing the inappropriate use of antibiotics) [12].

The materials with the potential for MVOCs and 3-methyl-1-butanol detection can be observed in the semiconducting metal oxides (SMOs), also applied for batteries [13,14], supercapacitors [15,16], and gas sensors [17,18]. Besides, there are two groups of SMOs: the n-type, such as ZnO [19], SnO_2 [20], and In_2O_3 [21], and the *p*-type such as Cr_2O_3[22], CuO [23], and NiO[24]. Cobalt oxide (Co_3O_4) is also a *p*-type SMO which has already been studied as a gas sensor [25–27]. However, most of the use of SMOs for gas sensing is based on *n*-type [28]. This fact can be explained by the undesired properties of *p*-type sensors, which include Co_3O_4, such as low selectivity, and high response time with low values. Thus, an alternative to improve these properties of pure SMOs is metal-organic frameworks (MOFs) as precursors for their synthesis. MOFs are three-dimensional structures containing the transition metal of interest between organic bonds, which exhibit a surface with greater porosity and morphology control [29,30]. For example, the zeolitic imidazole framework-8 (ZIF-8) is the MOF precursor for ZnO and has already been reported to present well-defined morphology and high performance as a gas sensor [31].

The *p-n* heterojunction between Co_3O_4 and ZnO is also an excellent mechanism for achieving suitable results in the sensing improvements of pure Co_3O_4 generated by the electronic transition in these materials [32–34]. Shi *et al*. [35] reported the synthesis of ZnO@Co_3O_4 hollow cubes by MOF as the precursor for high-response detection of toluene. Yan *et al*. [36] presented MOF-derived hollow Co_3O_4@ZnO cages applied for detection to 33 ppm of trimethylamine with good performance in sensitivity and low response/recovery time.

Doan *et al*. [37] synthesized ZnO/Co_3O_4 heterojunctions (ZIF-8/ZIF-67-derived) to detect low ethanol concentrations, varying the molar ratios. However, few articles report the use of heterojunction of Co_3O_4-ZnO for MVOC, especially for 3M1B detection, and the study of the metal molar ratio distribution's influence in the synthesis to upgrade the pure SMO sensing properties.

This present study improved the sensing properties of pure Co_3O_4 by synthesizing a ZIF-67-ZIF-8-derived heterostructure of Co_3O_4-ZnO for MVOC detection. The sensor measurements showed that the Co_3O_4-ZnO exhibits a suitable response for 3M1B in dry and controlled humid atmospheres, higher than Co_3O_4 and ZnO-Co_3O_4 samples. Furthermore, Co_3O_4-ZnO revealed an increase of more than two times in selectivity compared to pure Co_3O_4. In this case, a better sensing performance for 3M1B under different operation conditions was expressed by a *p-n* heterojunction of Co_3O_4-ZnO, containing a higher proportion of zinc in the material. This observation can be explained by the electronic transition in the *p-n* heterojunction process, increasing the number of active sites and facilitating oxygen adsorption on the surface.

3.2 Methods

3.2.1 Chemicals and materials

This work used reagents all purchased from Sigma-Aldrich with a high degree of purity (≥ 99%), including cobalt nitrate hexahydrate $Co(NO_3)_2.6H_2O$, zinc nitrate hexahydrate ($Zn(NO_3)_2.6H_2O$), and 2-methylimidazole (2-MI). The deionized (DI) water was purified through the Milli-Q setup (18.2 $M\Omega^{-1}$ at 25 °C, Millipore) for the synthesis.

3.2.2 Synthesis of pure Co_3O_4

According to previous work [35], the Co_3O_4 sample was prepared by synthesizing the MOF precursor (ZIF-67), followed by the calcination of this material. The ZIF-67 was synthesized using 290.7 mg $Co(NO_3)_2.6H_2O$, dissolved in 10 mL of DI water, and under stirring for 10 min. Subsequently, 4.54 g of 2-MIM was dissolved in 70 mL of DI water, added to the cobalt solution, and left at room temperature for 24 h. The product was centrifuged, washed with ethanol thrice, and dried at 55 °C overnight. To obtain the Co_3O_4 sample, the MOF was calcinated at 450 °C with a 2 °C min^{-1} heating rate for 2 h.

3.2.3 Synthesis of Co_3O_4-ZnO and ZnO-Co_3O_4 heterostructures

The MOF heterostructures synthesis was conducted using simple precipitation in two steps at room temperature. Initially, was produced the pure structure of ZIF-67 or ZIF-8. Secondly, a simple deposition of ZIF-8 or ZIF-67 was made above in the template solution to form the heterostructure, the details of which are described below. Firstly, the zinc solution was synthesized using $Zn(NO_3)_2.6H_2O$ (148.9 mg, 0.5 mmol), dissolved in 7 mL of DI water, and left under magnetic stirring for 10 min. After that, this solution was injected into the previously prepared 2-MI solution, which used 4.54 g of this ligand, dissolved in 70 mL DI water. Thus, this mixture was left under stirring for 30 min. Then, 7 mL of $Co(NO_3)_2.6H_2O$ aqueous solution (292.0 mg, 1 mmol) was included in the mixture, using a proportion of 0.5:1 mmol (zinc:cobalt), and the product was stood at room temperature for 24 h. The precipitate was collected by centrifuging, washed with ethanol/DI water three times, and dried at 55 °C overnight. The ZIF-67-ZIF-8 synthesis was very likely to ZIF-8-ZIF-67 but using a ratio of 0.5:1 mmol (cobalt:zinc), adding the zinc solution over the mixture of cobalt and 2-MI. Therefore, the ZnO-Co_3O_4 and Co_3O_4-ZnO were obtained by calcining both samples separately at 450 °C for 2 h with a heating rate of 2 °C min^{-1}.

Images of the synthesized samples are exhibited in Fig. 6., presenting a change in the color tone, especially in the MOFs, indicating the difference in the purple precipitate concentration of ZIF-67.

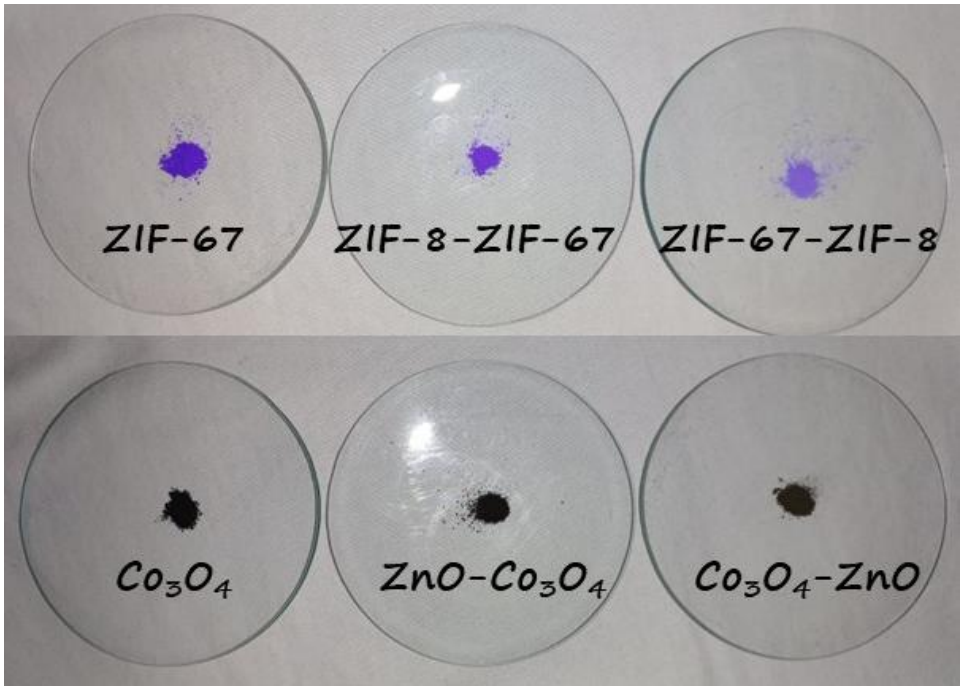

Fig. 6. Images of the synthesized samples in this study. Source: author.

3.2.4 Characterizations

X-ray diffraction (XRD) was used to investigate the crystal structure of the samples, operating a Rigaku model MiniFlex 300, using a Cu Kα radiation λ = 1.5418 Å, conducted at 30 kV and 10 mA. The measurements were recorded in the 5° to 80° range of the 2θ, with a step size of 0.01° and scanning rate of 1 ° min^{-1}. To acquire images of the samples and energy-dispersive X-ray (EDX) spectra, the field emission scanning electron microscopy (FESEM) technique was applied using an FEI Helios NanoLab 600i at 30 kV. The Brunauer-Emmett-Teller (BET) results of specific surface area were measured using a Micromeritics Gemini VII model 2390t. X-ray absorption spectroscopy (XAS) and X-ray photoelectron spectroscopy (XPS) measurements were conducted at the IPE beamline at Sirius, located at LNLS. The XPS was operated in kinetic energy at 400 eV and varying the photon energy, with incidence and takeoff angles being 45°, and the calibration of the spectra following the peak of C 1s (284.8 eV). A SPECS Phoibos 150 was used as an electron analyzer. The XAS measurements collected the total electron yield and fluorescence yield signals. The Fourier transform infrared spectroscopy (FTIR) was performed using a Perkin Elmer Spectrum Two spectrophotometer, operated in the 400-4000 cm^{-1} region with no heating process.

3.2.5 Sensor measurements and MVOC fabrication

The sensors were prepared with dispersions of the samples in isopropanol through the ultrasonic bath, depositing it 100 µL on alumina containing Au electrodes and heated for 1 h at 400 °C, as shown in Fig. 7. Subsequently, the sensor was placed in a tubular oven, under pure air flow (250 mL min^{-1}) to generate a clean atmosphere in the chamber. The resistance (R) of the pre-prepared electrodes was measured by applying a voltage of 5 V using a Keithley Source-Meter 2400.

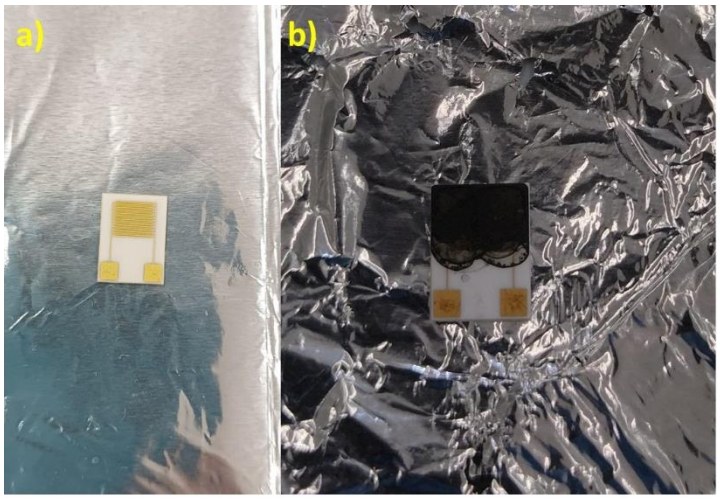

Fig. 7. Interdigitals containing Au electrodes on an alumina (a) before and (b) after the sample's suspension deposition. Source: author.

The preparation of MVOCs (3-methyl-1-butanol, 2-nonanone, acetone, ethanol, and ethyl acetate) was conducted using a calculus presented in Equation 1 to obtain the volumes of the reagents [38]:

$$C = \frac{22.4\rho TVs}{273MV} \times 1000 \quad (1)$$

where C is the concentration in ppm of the MVOC, ρ is the MVOC density (g ml^{-1}), T is the preparation temperature (K), Vs is the volume of MVOC liquid (µL), M is the molecular weight, and V is the preparation chamber volume (L).

To study humidity conditions in sensing measurements, saturated solutions of different salts were prepared. An Erlenmeyer containing the saturated solution was connected to the analysis chamber, with pure dry air passing through the solution before entering the chamber, carrying humidity. The relative humidity (R.H.) was monitored using a portable thermo-hygrometer HANNA, model HI 9564. The saturated salt solutions of K_2CO_3, NaBr, and NaCl were conducted for R.H. around 47, 65, and 83%, respectively.

The sensor measurements were made following the scheme shown in Fig. 8, injecting the MVOCs with individual syringes into the chamber. The responses for the selected MVOCs were calculated by the R_a (clean air resistance) ratio to R_{MVOC} (MVOC resistance) for the *n*-type sample and R_{MVOC} (MVOC resistance) ratio to R_a (clean air resistance) for the *p*-type samples. Thus, these quantifications were managed in different temperatures (190-350 °C) with dry and controlled humid atmospheres.

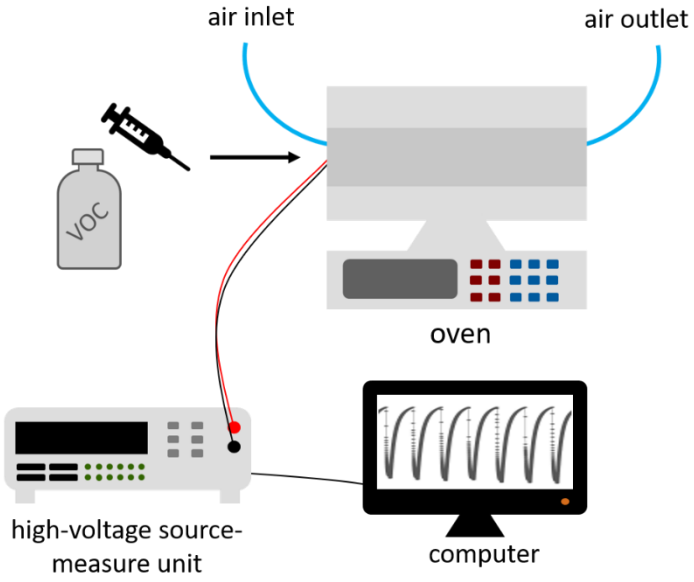

Fig. 8. Sensor measurements system scheme. Source: Bruna S. S. – Doctoral student and group partner.

3.3 Results and discussion

3.3.1 Materials characterization

The samples' synthesis process is summarized in Fig. 9. As discussed before, the Co_3O_4, Co_3O_4-Zno, and ZnO-Co_3O_4 were synthesized using precursors of MOFs. The ZIF-67, ZIF-67-ZIF-8, and ZIF-8-ZIF-67 were formed by a simple method at room temperature with their respective molar distributions, as shown in Fig. 9a-c. The morphology investigation of the samples was performed using a FESEM. Images of all MOF precursors are shown in Fig. S3, indicating a similar size and shape of polyhedral structures composed of ZIF-67 and ZIF-8 particles. Fig. 9d-f shows the MOF-derived samples Co_3O_4, Co_3O_4-ZnO, and ZnO-Co_3O_4 after calcination at 450 °C for 2h. The FESEM images of the oxides are shown in Fig. 9g-i, which maintained the polyhedral structure of the precursors but with the formation of a certain apparent roughness on the surface of these materials. The particles of the Co_3O_4 pure sample (Fig. 7g) were developed with a conglomerate structure, and the shape of heterostructures maintained the polyhedral formation. However, Fig. 9h,i shows the images of Co_3O_4-ZnO and ZnO-Co_3O_4, revealing a better polyhedral shape definition. A possible explanation for these observations is the heterostructure effect, in which the presence of zinc helped the particle's formation and maintained the results showed by the MOF precursor. Besides, the appearance of ZnO supports higher calcination temperatures than Co_3O_4, presenting differences in the thermodynamic properties.

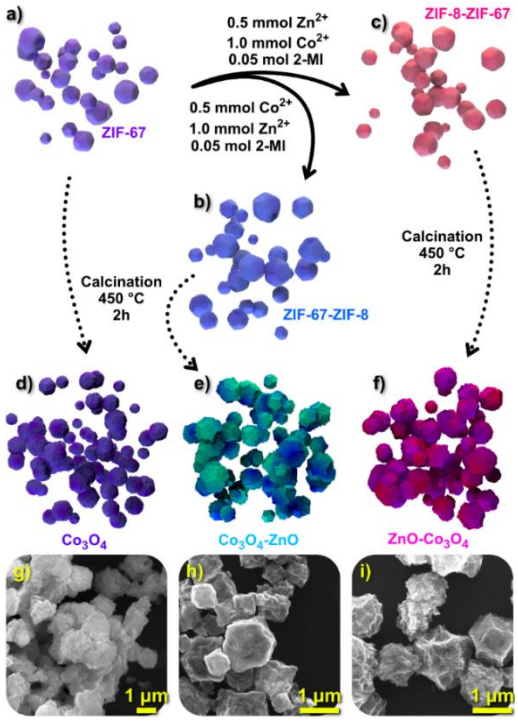

Fig. 9. Summary of the MOF synthesis processes of (a) ZIF-67, (b) ZIF-67-ZIF-8, and (c) ZIF-8-ZIF-67. Oxides samples representations of (d) Co_3O_4, (e) Co_3O_4-ZnO, and (f) ZnO-Co_3O_4. FESEM images of (g) Co_3O_4, (h) Co_3O_4-ZnO, and (i) ZnO-Co_3O_4. Source: Tarcísio M. P. – group partner.

XRD data of the synthesized materials are shown in Fig. 10 for crystalline structure analysis. The diffraction results of the precursor ZIF-67 in Fig. 10a match those of the literature pattern [39]. Furthermore, for samples ZIF-8-ZIF-67 and ZIF-67-ZIF-8, their diffraction patterns are similar to those of the reported ZIF-67. As for the diffraction patterns of ZIF-67-derived Co_3O_4 shown in Fig. 10b, the peaks are compatible with the standard cubic phase of Co_3O_4 (JCPDS: 80-1532), and no other secondary peaks are observed, indicating a single-phase system. The ZnO-Co_3O_4 and Co_3O_4-ZnO materials exhibit diffraction patterns compatible with both the Co_3O_4 sample and the hexagonal ZnO (JCPDS: 89-510), revealing the existence of zinc and cobalt phases and the formation of heterostructures with the absence of spurious phases.

The investigation of the functional groups in the materials was conducted by FTIR analysis. The spectra of the ZIF-67-ZIF-8, ZIF-8-ZIF-8, and ZIF-67 are viewed in Fig 10c, exhibiting similar profiles. The band located at 2981 cm^{-1} corresponds to the C-H stretching vibration, and the ones with the maximum at 1581 cm^{-1} and 1424 cm^{-1}, in turn, are attributed to the C=N bond and the C-H stretching in CH_2, respectively [40]. The band centered at 1144 cm^{-1} indicates the existence of imidazolate, formed by imidazole transformation [41]. The Co-N or Zn-N bonds can be assigned to the large band at 421 cm^{-1}. In the spectra of Co_3O_4-ZnO, ZnO-Co_3O_4 and Co_3O_4, Fig. 10d, all samples exhibit a band around 665 cm^{-1}, but the band at 558 cm^{-1} is detected only for the more Co molar concentration samples (ZnO-Co_3O_4 and Co_3O_4), which is associated with the Co-O bond due to the presence of Co_3O_4 [61]. Furthermore, it is possible to observe a drop in transmittance in the region of 400 cm^{-1} in the heterostructures, showing the presence of Zn-O stretching [42]. The non-observation of other absorption bands in the IR indicates that all organic matter was eliminated in the calcination stage.

The pore size distribution and specific surface area of the materials are summarized in Table 1. As for the BET results for ZIF-67, ZIF-8-ZIF-67 and ZIF-67-ZIF-8, these samples exhibit high specific surface areas of 878.1, 1156.2 and 985.3 $m^2\ g^{-1}$ and large pore volumes of 0.457, 0.597 and 0.521 cm^3/g, respectively, indicating materials of porous nature. After the calcination step, the BET results for Co_3O_4, ZnO-Co_3O_4 and Co_3O_4-ZnO indicate a significant decrease in their specific surface area and pore volumes. However, an increase in average pore size was observed in these samples. Furthermore, comparing only between the synthesized SMOs, ZnO-Co_3O_4 presents a higher specific surface area of 22.4 $m^2\ g^{-1}$, compared to Co_3O_4 (20.5 $m^2\ g^{-1}$) and Co_3O_4-ZnO (14.6 $m^2\ g^{-1}$). Finally, Fig. 10e and Fig. 10f demonstrate the nitrogen adsorption/desorption isotherms of MOFs and oxides, respectively, with similar

profiles. These results are essential to discuss the diffusion and reaction of gases in the sensor mechanism involving their materials, caused by surface reactions.

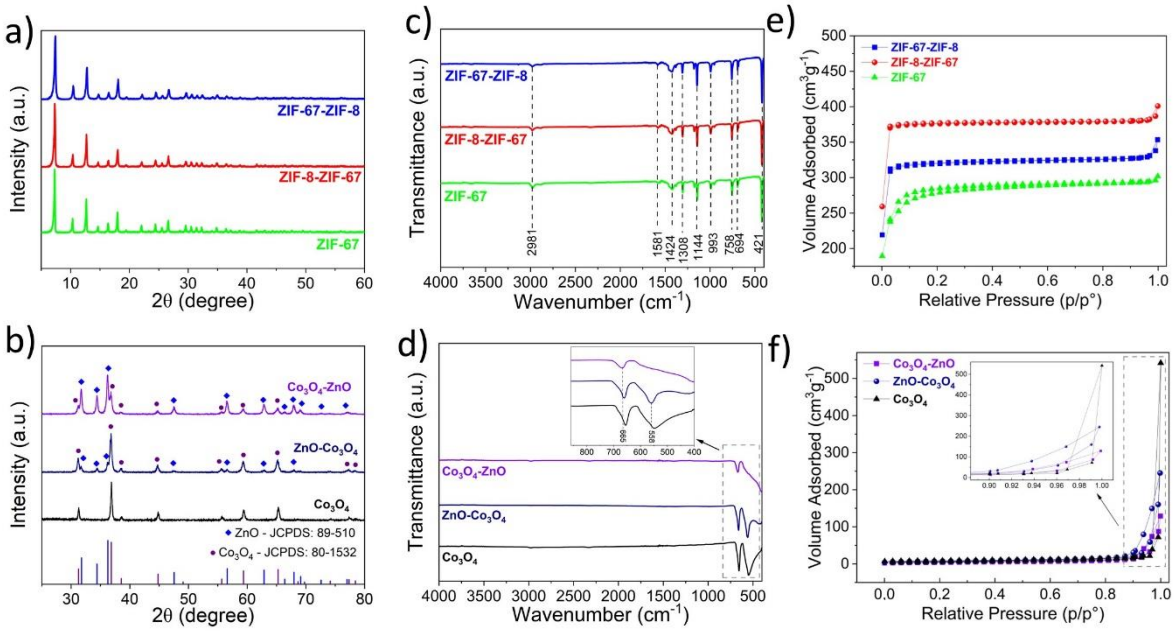

Fig. 10. XRD patterns of (a) ZIF-67, ZIF-8-ZIF-67, ZIF-67-ZIF-8 (b) Co_3O_4, ZnO-Co_3O_4, and Co_3O_4-ZnO. FTIR spectra of (c) ZIF-67, ZIF-8-ZIF-67, ZIF-67-ZIF-8, (d) Co_3O_4, ZnO-Co_3O_4, and Co_3O_4-ZnO. Isotherms by nitrogen adsorption and desorption of (e) ZIF-67, ZIF-8-ZIF-67, ZIF-67-ZIF-8, (f) Co_3O_4, ZnO-Co_3O_4, and Co_3O_4-ZnO. Source: author

Table 1
Surface area, pore size, and pore volume comparison among all the synthesized materials in this work.

Material	Surface area (m^2 g^{-1})	Pore size (nm) [a]	Pore volume (cm^3/g) [b]
ZIF-67	878.1	2.1	0.457
ZIF-8-ZIF-67	1156.2	2.1	0.597
ZIF-67-ZIF-8	985.3	2.1	0.521
Co_3O_4	20.5	21.2	0.108
ZnO-Co_3O_4	22.4	41.9	0.235
Co_3O_4-ZnO	14.6	32.4	0.118

[a] Adsorption average pore diameter (4V/A by BET); [b] Single point adsorption total pore volume of pores less than 1952.438 Å width at p/p° = 0.9900000. Source: author

EDX technique was used for elemental analysis and to investigate the Zn and Co distribution in the heterostructure particles, as shown in Fig. 11. The EDX analysis of ZnO-Co_3O_4 and Co_3O_4-ZnO are illustrated in Fig. 11a-b, respectively, containing X-ray emission peaks of C, O, Co, and Zn. The peak of C is from the carbon tape used in the sample holder during the analysis. No other emissions peaks are shown, proving the nonexistence of impurities in both samples. The FESEM images representing the region of EDX analysis for ZnO-Co_3O_4 and Co_3O_4-ZnO are shown in Fig. 11c-d, respectively. The Zn and Co atoms distribution in the particles is uniform in both samples, as represented in Fig. 11e-h, following their respective molar proportions.

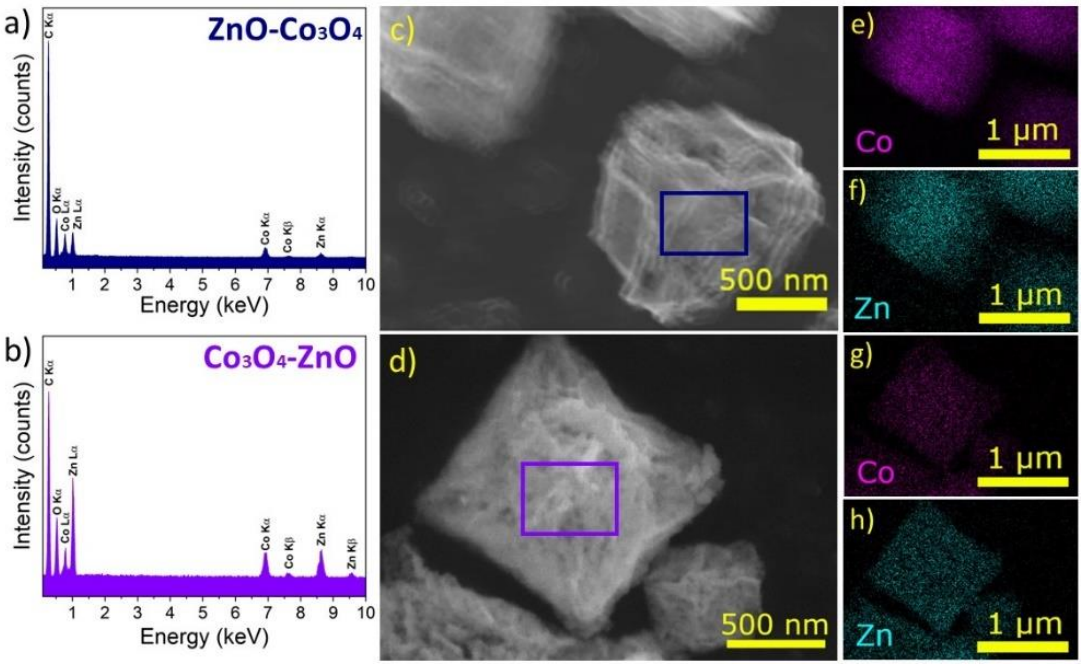

Fig. 11. Elemental analysis with EDX spectra of (a) ZnO-Co_3O_4, and (b) Co_3O_4-ZnO. FESEM images of EDX region of (c) ZnO-Co_3O_4, and (d) Co_3O_4-ZnO. EDX mapping images of (e-f) ZnO-Co_3O_4, and (g-h) Co_3O_4-ZnO. Source: author

XPS performed the oxidation states of the elements and chemical analysis on the surfaces. The survey spectra of Co_3O_4, ZnO-Co_3O_4, and Co_3O_4-ZnO are demonstrated in Fig. 12a, indicating that the materials are composed of Zn (except for Co_3O_4), Co, O, and C. The presence of C is related to the adsorption of CO_2 from the atmosphere. Other peaks are not revealed in this inspection. The Co *2p* high-resolution XPS of the Co_3O_4-ZnO is viewed in Fig. 12b, exhibiting two peaks located at 782.1 (Co $2p_{3/2}$) eV and 797.7 eV (Co $2p_{1/2}$) [43]. The distance between these peaks is about 15.6 eV, confirming the presence of Co_3O_4 in the material [44]. Moreover, the two peaks could be deconvoluted into four sub-peaks: two representing Co^{2+} (783.4 eV and 798.6 eV) and the other two related to Co^{3+} (781.7 eV and 796.9 eV) [45]. Zn 2*p* high-resolution spectrum is illustrated in Fig. 12c, showing two peaks centered at 1023 eV (Zn $2p_{3/2}$) and 1046.2 eV (Zn $2p_{1/2}$) [46], with a difference of 23.2 eV, revealing the presence of Zn^{2+} by ZnO. Finally, the O 1s high-resolution spectrum (Fig. 12d) indicates a peak centered at 531.2 eV, with a deconvolution showing two sub-peaks at 531.1 eV and 531.9 eV. The peak at 531.1 eV can be associated with lattice oxygen (O^{2-}), and the region at 531.9 eV can be related to adsorbed oxygen [47]. The high-resolution of the ZnO-Co_3O_4 (Fig. S1a-c) and Co_3O_4 (Fig. S1d and Fig. S1e) presented similar characteristics. However, differences in the peak intensities at 783.4 eV for the high-resolution Co 2*p* are observed, revealing a higher Co^{2+} state concentration in Co_3O_4 than ZnO-Co_3O_4 and Co_3O_4-ZnO.

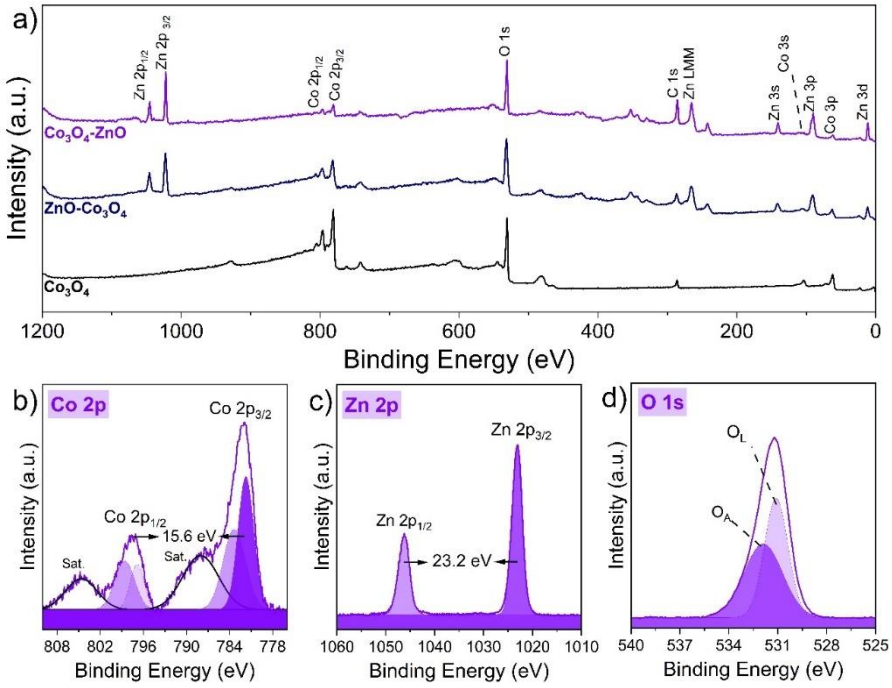

Fig. 12. (a) XPS survey scan spectra of Co_3O_4, ZnO-Co_3O_4, and Co_3O_4-ZnO. High-resolution XPS spectra from (b) Co 2p, (c) Zn 2p, and O 1s of the Co_3O_4-ZnO. Source: author

The XAS at total electron yield (TEY) mode was conducted to study the valence states and atomic structures. The spectra at Co $L_{2,3}$-edge of the materials are exihibited in Fig. 13a, and the peaks centered at the 780 and 795 eV region are related to L_3 and L_2, respectively. The Co L_3-edge region presents a significant peak (1) at 780.8 eV, indicating the existence of Co^{3+}, and a minor peak (2) at 779.5 eV representing the Co^{2+} species [48,49]. So, a mixture of two different valence states of Co is demonstrated in the synthesized materials, and this distribution can be estimated by the ratio of Co^{3+}/Co^{2+} represented by 2/1 peaks. The calculated ratios are 2.77, 2.70, and 1.75 for Co_3O_4-ZnO, ZnO-Co_3O_4, and Co_3O_4, respectively. In other words, the Co^{2+} concentration decreased with increasing Zn^{2+} concentration in the heterostructures, favoring the stabilization of Co^{3+} ions. These observations are in harmony with the XPS discussed before.

Fig. 13b shows the XAS spectra at the Zn $L_{2,3}$-edge of the Co_3O_4-ZnO and ZnO-Co_3O_4 samples. The peaks at the 1-3 region represent the L_3-edge. These peaks are centered at 1023, 1027.7, and 1033.6 eV, respectively, revealing the electronic transition of Zn 2*p* to the Zn 4*s* and 3*d* states [50,51].

The XAS analysis at the O K-edge of the Co_3O_4-ZnO, ZnO-Co_3O_4, and Co_3O_4 are shown in Fig. 13c. The peak 1 with 530.9 eV of binding energy demonstrates the hybridized O species with low-spin Co^{3+} states [52]. Furthermore, the Co_3O_4-ZnO and ZnO-Co_3O_4 present higher intensities peaks at 538 eV (peak 2) than Co_3O_4, suggesting the Co^{2+} decreasing by the reduction

of the electronic transition of 3*s* and 3*p* to empty states [49], as described in Co $L_{3,2}$-edge discussion.

As for the XAS spectra at total fluorescent yield (TFY) mode shown in Fig. S2a-c, the samples showed the same characteristics as the TEY described above.

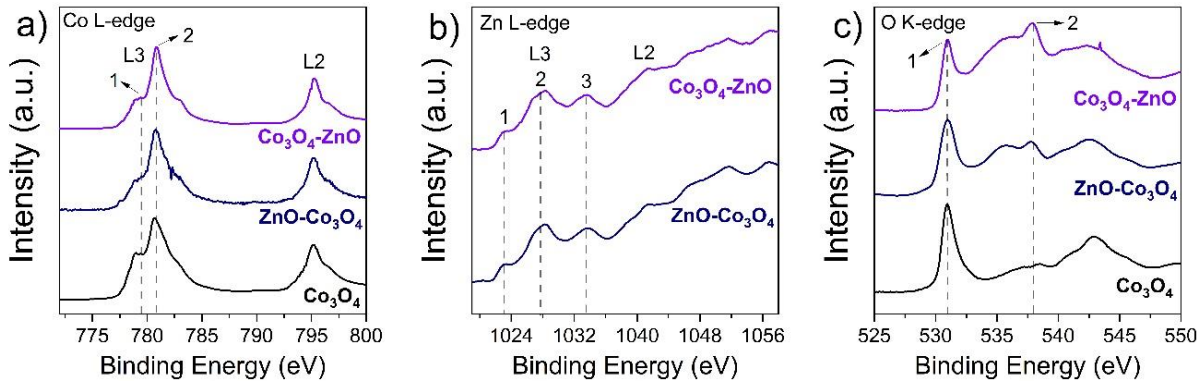

Fig. 13. XAS spectra in TEY around the (a) Co, (b) Zn, and (c) O K-edges of the Co_3O_4, ZnO-Co_3O_4, and Co_3O_4-ZnO. Source: author

3.3.2 MVOCs sensing measurements

The electrical measurements analyzed the MVOC sensor properties of Co_3O_4, ZnO-Co_3O_4, and Co_3O_4-ZnO in different operation conditions, such as temperature range from 190 °C to 350 °C. No significant results were observed below 190 °C. Moreover, the Co_3O_4-ZnO measurements were also conducted in an atmosphere with controlled relative humidity (47, 65, and 83% R.H.), using saturated salt solutions, to study the possible effects on the selectivity of this sensor.

The MVOCs selected were measured at 100 ppm to verify the selectivity in the optimal operating temperature of the sensors (Fig. 14a). In this way, the higher MVOC responses are noticed at 230 °C for the ZnO-Co_3O_4 and at 270 °C for the Co_3O_4-ZnO, and Co_3O_4, showing their optimal temperature. The 3M1B responses in the function of temperature are shown in Fig. 14b, demonstrating a better response of 14.6 to the heterostructure Co_3O_4-ZnO at 270 °C, higher than the 5.9 of ZnO-Co_3O_4 and 8.4 of Co_3O_4. As for the selectivity of the sensors, Fig. 14c shows a radar graph with a ratio of 3M1B responses to the second-best MVOC measured, indicating a selectivity of 2.79 to Co_3O_4-ZnO, twice that of Co_3O_4 with 1.34. In other words, the heterojunction improved the selectivity of the pure sample at the optimal temperature, a crucial factor for MVOC sensors. The Co_3O_4-ZnO responses at 270 °C in different concentrations of 3M1B are summarized in Fig. 14d, exhibiting the MVOC detection in low concentrations, such as 2 and 5 ppm. However, the sensor has been saturated in high

concentrations of 3M1B, maintaining the same response from 100 to 500 ppm. The response time was calculated based on 90% of the peak resistance after the insertion of MVOC. As for the recovery time, it is the time to recover 90% of the initial baseline. These results are shown in Fig. 14e, demonstrating a response and recovery time of 11.4 s and 879.1 s, respectively. The time for response of Co_3O_4-ZnO obtained was faster in the three synthesized samples. Co_3O_4 presents a response time of 14.6 s and 23.9 s for the ZnO-Co_3O_4. On the other hand, the recovery time of 879.1 s is the slowest compared to the other synthesized sensors. The repeatability measurements were conducted 15 times for 10 ppm of 3M1B at 270 °C in dry air (Fig. 14f), exhibiting an average response of 2.79 ± 0.29. So, it can be observed that there is excellent stability in the continuous use for 3M1B detection, keeping the response values during the process essential to the life cycle of the sensor.

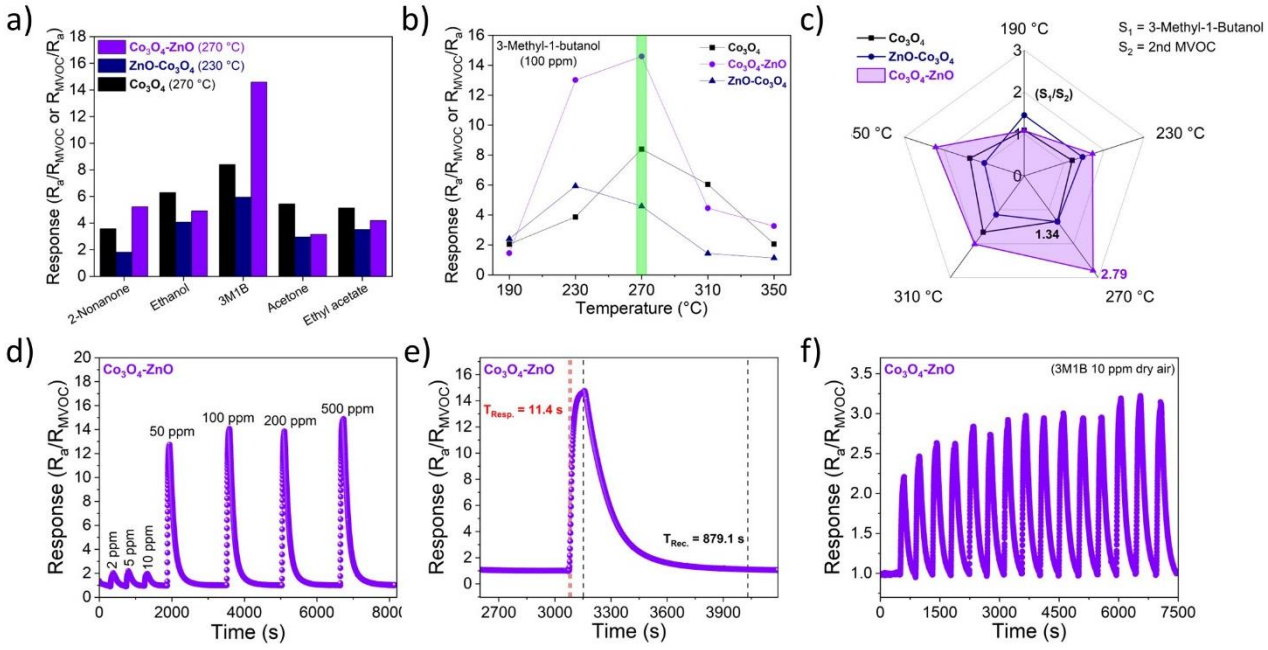

Fig. 14. Co_3O_4, ZnO-Co_3O_4, and Co_3O_4-ZnO sensor measurements in dry atmosphere for (a) selectivity to 100 ppm of different MVOCs at respectively optimum temperature, (b) responses to 100 ppm of 3M1B as a function of temperature, and (c) radar graph for selectivity ratio to 3M1B. Co_3O_4-ZnO performance measurements in dry atmosphere for 3M1B at 270 °C in (d) different concentrations, (e) response and recovery time to 100 ppm, and (f) sensor repeatability to 10 ppm. Source: author

To study the influence of humidity on the Co_3O_4-ZnO sensor, different MVOCs with a concentration of 100 ppm were tested at the optimal temperature of 270 °C at 47, 65, and 83% R.H. These results are shown in Fig. 15, revealing a slight decrease in the responses compared to the dry atmosphere. Furthermore, the measurements of 65% R.H. showed a response of 10.42, higher than the other humidity conditions. The selectivity for the 3-methyl-1-butanol was still maintained in humid conditions, demonstrating good sensing properties in real

working conditions. However, the responses are generally reduced in these circumstances but still present good results for 3M1B detection, mainly for the measurements at 65% R.H.

The increase in the sensing properties observed for the Co_3O_4-ZnO, compared to pure Co_3O_4, can be justified by the electronic changes caused by the *p-n* heterojunction. This way, the active sites and the stable depletion layer can explain the higher sensor results. Besides, the measurements obtained for the Co_3O_4 were conducted following the present method, maintaining a standard of comparison between the synthesized samples in this study.

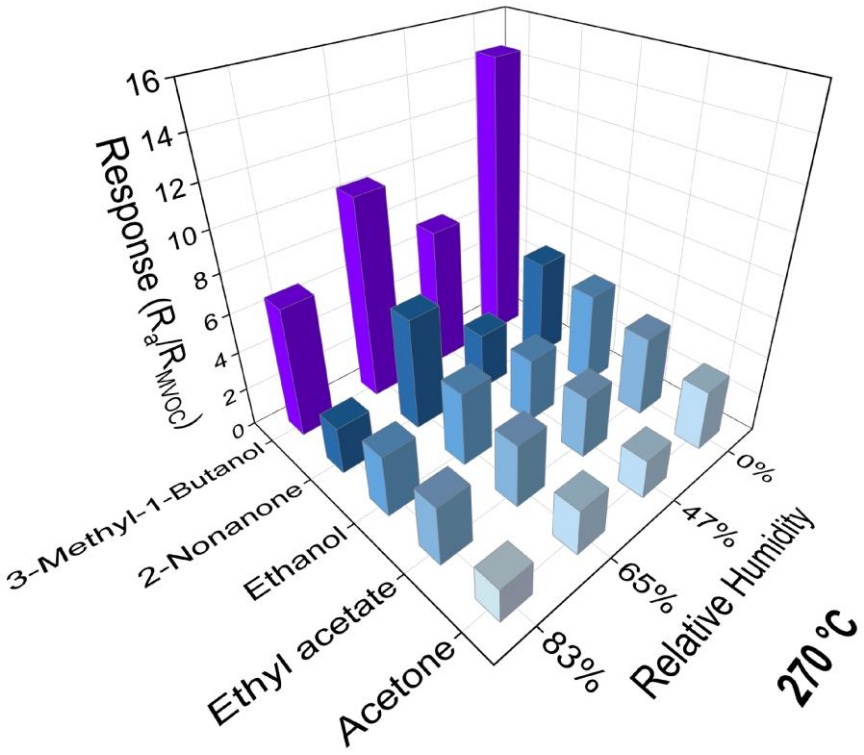

Fig. 15. Co_3O_4-ZnO sensor responses at 270 °C to 100 ppm for different MVOCs in dry and controlled humid atmospheres. Source: author.

3.4 3-methyl-1-butanol sensing mechanism

As discussed in section 1.2.2, the mechanism for SMOs applied as MVOC and gas sensors is established on the adsorbed oxygen reaction on the surface of the material. Besides, different oxygen species are related to the operation temperature. A plausible explanation for the 3-methyl-1-butanol mechanism is the oxidation process at the material's surface when exposed to an air atmosphere, increasing the electron density, and consuming the electrons from the conducting band. In this way, the 3M1B detection is facilitated, and when the sensor is in contact with this MVOC, the target volatile reacts with the adsorbed oxygen, releasing electrons, CO_2, and water molecules, according to the Eq. 2 [53]:

$$2C_5H_{12}O + 15O_2^{-}{}_{(ads)} \rightarrow 10CO_{2\,(gas)} + 12H_2O_{\,(gas)} + 15e^{-} \qquad (2)$$

The sensor response is calculated by the decrease in the material's resistance when in contact with the 3M1B. This process in an *n*-type SMO is caused by the released electrons turning back to the conducting band of the material, as shown in Fig. 16. As for the *p*-type sensors, the resistance increases when the emitted electrons recombine with the holes at the valence band after the 3M1B contact. In both cases, it returns to the initial stage with the species desorption process at the surface and conducting to the air resistance value, also called the reversibility of the sensor.

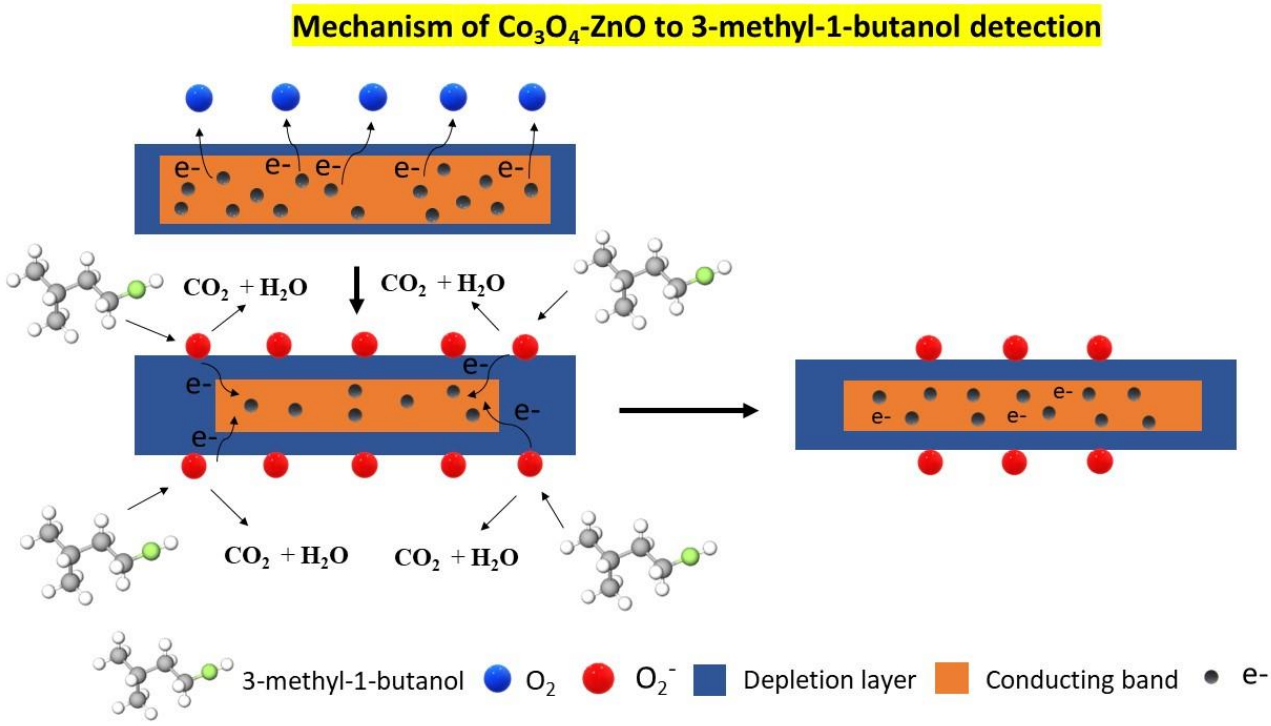

Fig. 16. *n*-type sensing mechanism of Co_3O_4-ZnO to 3-methyl-1-butanol detection. Source: author.

5 CONCLUSIONS

In summary, we developed an improved material by a simple MOF-derived synthesis with ZnO and Co_3O_4, forming a heterostructure to apply as an MVOC sensor. The Co_3O_4-ZnO showed a higher response of 14.6 to 100 ppm of 3-methyl-1-butanol at 270 °C, with a selectivity ratio of 2.79 and 11.4 s response time in dry air. Furthermore, it was possible to obtain a response of 10.42 to 3M1B in a humid atmosphere of 65% R.H. In other words, this sensor revealed a significant upgrade in sensing properties compared to pure Co_3O_4 with a response of 8.4 to 3M1B, using the present standard method for comparison.

The high sensing performance shown by Co_3O_4-ZnO can be related to the *p-n* heterojunction effect. As discussed in the BET results, the Co_3O_4-ZnO presented a lower specific surface area than the other samples. However, this heterostructure obtained higher sensing responses, indicating that the *p-n* heterojunction was crucial for the sensor performance. This synthesis process changes the characteristics of the cobalt semiconductor, upgrading the pure Co_3O_4 properties by forming a two-phase material with the ZnO. In addition, this composite presented great attributes for detecting MVOCs, especially for 3M1B. So, this work presented material with a barely studied application, a simple synthesis process, and the capability of working in different operation conditions.

CRediT authorship contribution statement

Gustavo S. M. Santos: investigation, methodology, data curation, writing - original draft. Bruna S. de Sá: investigation, methodology, writing – review & editing. Tarcísio M. Perfecto: investigation, software, graphic design, writing - review & editing. Diogo P. Volanti: conceptualization, project administration, funding acquisition, supervision, writing - review & editing.

ACKNOWLEDGMENT

This work was supported by Coordination for the Improvement of Higher Education Personnel (CAPES) (grant number 88887.649732/2022-0), São Paulo Research Foundation (FAPESP) (grant numbers 2020/05233-7 and 2020/06421-1). XRD and FTIR were supplied by LSQA/IBILCE/UNESP. FESEM and EDX were supplied by LME-IQ-UNESP. We also thank Felipe de Souza Custódio, Thiago José de Almeida Mori and Tulio Costa Rizuti da Rocha for the XPS and XAS, located at IPE beamline on Sirius-LNLS (proposal 20221938).

References

[1] A. Korpi, J. Järnberg, A.L. Pasanen, Microbial volatile organic compounds, Crit Rev Toxicol. 39 (2009) 139–193. https://doi.org/10.1080/10408440802291497.

[2] L. Weisskopf, S. Schulz, P. Garbeva, Microbial volatile organic compounds in intra-kingdom and inter-kingdom interactions, Nat Rev Microbiol. 19 (2021) 391–404. https://doi.org/10.1038/s41579-020-00508-1.

[3] P. Gao, F. Korley, J. Martin, B.T. Chen, Determination of Unique Microbial Volatile Organic Compounds Produced by Five Aspergillus Species Commonly Found in Problem Buildings, AIHA Journal. 63 (2002) 135–140. https://doi.org/10.1080/15428110208984696.

[4] Y. Wang, Y. Li, J. Yang, J. Ruan, C. Sun, Microbial volatile organic compounds and their application in microorganism identification in foodstuff, TrAC - Trends in Analytical Chemistry. 78 (2016) 1–16. https://doi.org/10.1016/j.trac.2015.08.010.

[5] E. Duffy, A. Morrin, Endogenous and microbial volatile organic compounds in cutaneous health and disease, TrAC - Trends in Analytical Chemistry. 111 (2019) 163–172. https://doi.org/10.1016/j.trac.2018.12.012.

[6] A.D. Wilson, Advances in electronic-nose technologies for the detection of volatile biomarker metabolites in the human breath, Metabolites. 5 (2015) 140–163. https://doi.org/10.3390/metabo5010140.

[7] S. Garcia-Alcega, Z.A. Nasir, R. Ferguson, C. Whitby, A.J. Dumbrell, I. Colbeck, D. Gomes, S. Tyrrel, F. Coulon, Fingerprinting outdoor air environment using microbial volatile organic compounds (MVOCs) – A review, TrAC - Trends in Analytical Chemistry. 86 (2017) 75–83. https://doi.org/10.1016/j.trac.2016.10.010.

[8] Y. Fan, K.R. Schneider, P.J. Sarnoski, Determining spoilage of whiteleg shrimp (Litopanaeus vannemei) during refrigerated storage using colorimetric strips, Food Chem X. 14 (2022). https://doi.org/10.1016/j.fochx.2022.100263.

[9] L. Ernstgård, D. Norbäck, T. Nordquist, G. Wieslander, R. Wålinder, G. Johanson, Acute effects of exposure to vapors of 3-methyl-1-butanol in humans, Indoor Air. 23 (2013) 227–235. https://doi.org/10.1111/ina.12002.

[10] S. Samanta, P. Srinivasan, J.B.B. Rayappan, K. Kailasam, Ru quantum dots decorated graphitic carbon nitride (Ru-QDs@g-CN) for chemi-resistive sensing of 3-methyl-1-butanol at room temperature, Sens Actuators B Chem. 368 (2022). https://doi.org/10.1016/j.snb.2022.132060.

[11] G.C.N. Vioto, T.M. Perfecto, C.A. Zito, D.P. Volanti, Flower-like NiO for the detection of 3-methyl-1-butanol, a microbial volatile organic compound, Mater Lett. 333 (2023). https://doi.org/10.1016/j.matlet.2022.133641.

[12] K.E. Fleming-Dutra, A.L. Hersh, D.J. Shapiro, M. Bartoces, E.A. Enns, T.M. File, J.A. Finkelstein, J.S. Gerber, D.Y. Hyun, J.A. Linder, R. Lynfield, D.J. Margolis, L.S. May, D. Merenstein, J.P. Metlay, J.G. Newland, J.F. Piccirillo, R.M. Roberts, G. V. Sanchez, K.J. Suda, A. Thomas, T.M. Woo, R.M. Zetts, L.A. Hicks, Prevalence of inappropriate

antibiotic prescriptions among us ambulatory care visits, 2010-2011, JAMA - Journal of the American Medical Association. 315 (2016) 1864–1873. https://doi.org/10.1001/jama.2016.4151.

[13] D. Santos-Carballal, O. Lupan, N. Magariu, N. Ababii, H. Krüger, M.T. Bodduluri, N.H. de Leeuw, S. Hansen, R. Adelung, Al2O3/ZnO composite-based sensors for battery safety applications: An experimental and theoretical investigation, Nano Energy. 109 (2023). https://doi.org/10.1016/j.nanoen.2023.108301.

[14] M. Dotoli, R. Rocca, M. Giuliano, G. Nicol, F. Parussa, M. Baricco, A.M. Ferrari, C. Nervi, M.F. Sgroi, A Review of Mechanical and Chemical Sensors for Automotive Li-Ion Battery Systems, Sensors. 22 (2022). https://doi.org/10.3390/s22051763.

[15] S. Sivakumar, Y. Robinson, N.A. Mala, Studies on photocatalytic performance and supercapacitor applications of undoped and Cu-doped ZnO nanoparticles, Applied Surface Science Advances. 12 (2022). https://doi.org/10.1016/j.apsadv.2022.100344.

[16] J. Zhi, M. Zhou, Z. Zhang, O. Reiser, F. Huang, Interstitial boron-doped mesoporous semiconductor oxides for ultratransparent energy storage, Nat Commun. 12 (2021). https://doi.org/10.1038/s41467-020-20352-4.

[17] K.G. Krishna, S. Parne, N. Pothukanuri, V. Kathirvelu, S. Gandi, D. Joshi, Nanostructured metal oxide semiconductor-based gas sensors: A comprehensive review, Sens Actuators A Phys. 341 (2022). https://doi.org/10.1016/j.sna.2022.113578.

[18] M.V. Nikolic, V. Milovanovic, Z.Z. Vasiljevic, Z. Stamenkovic, Semiconductor gas sensors: Materials, technology, design, and application, Sensors (Switzerland). 20 (2020) 1–31. https://doi.org/10.3390/s20226694.

[19] F. Meng, X. Shi, Z. Yuan, H. Ji, W. Qin, Y.B. Shen, C. Xing, Detection of four alcohol homologue gases by ZnO gas sensor in dynamic interval temperature modulation mode, Sens Actuators B Chem. 350 (2022). https://doi.org/10.1016/j.snb.2021.130867.

[20] Y. Masuda, Recent advances in SnO2 nanostructure based gas sensors, Sens Actuators B Chem. 364 (2022). https://doi.org/10.1016/j.snb.2022.131876.

[21] S. Yang, H. Yin, Z. Wang, G. Lei, H. Xu, Z. Lan, H. Gu, Gas sensing performance of In2O3 nanostructures: A mini review, Front Chem. 11 (2023). https://doi.org/10.3389/fchem.2023.1174207.

[22] B.Y. Song, L.H. Liu, M. Yang, X.F. Zhang, Z.P. Deng, Y.M. Xu, L.H. Huo, S. Gao, Biotemplate-directed synthesis of Cr2O3 mesoporous monotubes for enhanced sensing to trace H2S gas, Sens Actuators B Chem. 369 (2022). https://doi.org/10.1016/j.snb.2022.132294.

[23] H. Bai, H. Guo, J. Wang, Y. Dong, B. Liu, Z. Xie, F. Guo, D. Chen, R. Zhang, Y. Zheng, A room-temperature NO2 gas sensor based on CuO nanoflakes modified with rGO nanosheets, Sens Actuators B Chem. 337 (2021). https://doi.org/10.1016/j.snb.2021.129783.

[24] T.P. Mokoena, H.C. Swart, K.T. Hillie, Z.P. Tshabalala, M. Jozela, J. Tshilongo, D.E. Motaung, Enhanced propanol gas sensing performance of p-type NiO gas sensor

induced by exceptionally large surface area and crystallinity, Appl Surf Sci. 571 (2022). https://doi.org/10.1016/j.apsusc.2021.151121.

[25] J.M. Xu, J.P. Cheng, The advances of Co3O4as gas sensing materials: A review, J Alloys Compd. 686 (2016) 753–768. https://doi.org/10.1016/j.jallcom.2016.06.086.

[26] X. Fan, Y. Xu, C. Ma, W. He, In-situ growth of Co3O4 nanoparticles based on electrospray for an acetone gas sensor, J Alloys Compd. 854 (2021). https://doi.org/10.1016/j.jallcom.2020.157234.

[27] G.W.C. Kumarage, E. Comini, Low-dimensional nanostructures based on cobalt oxide (Co3o4) in chemical-gas sensing, Chemosensors. 9 (2021). https://doi.org/10.3390/chemosensors9080197.

[28] H.J. Kim, J.H. Lee, Highly sensitive and selective gas sensors using p-type oxide semiconductors: Overview, Sens Actuators B Chem. 192 (2014) 607–627. https://doi.org/10.1016/j.snb.2013.11.005.

[29] Y.V. Kaneti, J. Tang, R.R. Salunkhe, X. Jiang, A. Yu, K.C.W. Wu, Y. Yamauchi, Nanoarchitectured Design of Porous Materials and Nanocomposites from Metal-Organic Frameworks, Advanced Materials. 29 (2017). https://doi.org/10.1002/adma.201604898.

[30] W. Xia, A. Mahmood, R. Zou, Q. Xu, Metal-organic frameworks and their derived nanostructures for electrochemical energy storage and conversion, Energy Environ Sci. 8 (2015) 1837–1866. https://doi.org/10.1039/c5ee00762c.

[31] X. Zhang, W. Lan, J. Xu, Y. Luo, J. Pan, C. Liao, L. Yang, W. Tan, X. Huang, ZIF-8 derived hierarchical hollow ZnO nanocages with quantum dots for sensitive ethanol gas detection, Sens Actuators B Chem. 289 (2019) 144–152. https://doi.org/10.1016/j.snb.2019.03.090.

[32] X. Wang, B. Yang, Y. Wang, G. Yi, T. Wang, J. Zhou, Z. Zhang, Preparation of porous Co3O4-ZnO nanosheet composites and study of their gas-sensitive properties, Journal of Porous Materials. (2023). https://doi.org/10.1007/s10934-023-01476-6.

[33] X. Fan, S. Yang, C. Huang, Y. Lu, P. Dai, Preparation and Enhanced Acetone-Sensing Properties of ZIF-8-Derived Co3O4@ZnO Microspheres, Chemosensors. 11 (2023) 376. https://doi.org/10.3390/chemosensors11070376.

[34] S. Yang, G. Lei, H. Xu, Z. Lan, Z. Wang, H. Gu, Metal oxide based heterojunctions for gas sensors: A review, Nanomaterials. 11 (2021). https://doi.org/10.3390/nano11041026.

[35] J. Shi, J. Xiong, L. Qiao, C. Liu, Y. Zeng, Facile MOF-on-MOF isomeric strategy for ZnO@Co3O4 single-shelled hollow cubes with high toluene detection capability, Appl Surf Sci. 609 (2023) 155271. https://doi.org/10.1016/j.apsusc.2022.155271.

[36] W. Yan, H. Xu, M. Ling, S. Zhou, T. Qiu, Y. Deng, Z. Zhao, E. Zhang, MOF-Derived Porous Hollow Co3O4@ZnO Cages for High-Performance MEMS Trimethylamine Sensors, ACS Sens. 6 (2021) 2613–2621. https://doi.org/10.1021/acssensors.1c00315.

[37] T.L.H. Doan, J.Y. Kim, J.H. Lee, L.H.T. Nguyen, Y.T. Dang, K.B.T. Bui, A.T.T. Pham, A. Mirzaei, T.B. Phan, S.S. Kim, Preparation of n-ZnO/p-Co3O4 heterojunctions from zeolitic imidazolate frameworks (ZIF-8/ZIF-67) for sensing low ethanol concentrations, Sens Actuators B Chem. 348 (2021). https://doi.org/10.1016/j.snb.2021.130684.

[38] D. Zhang, A. Liu, H. Chang, B. Xia, Room-temperature high-performance acetone gas sensor based on hydrothermal synthesized SnO2-reduced graphene oxide hybrid composite, RSC Adv. 5 (2015) 3016–3022. https://doi.org/10.1039/c4ra10942b.

[39] A.F. Gross, E. Sherman, J.J. Vajo, Aqueous room temperature synthesis of cobalt and zinc sodalite zeolitic imidizolate frameworks, Dalton Transactions. 41 (2012) 5458–5460. https://doi.org/10.1039/c2dt30174a.

[40] H. Beitollahi, M. Shahsavari, I. Sheikhshoaie, S. Tajik, P.M. Jahani, S.Z. Mohammadi, A.A. Afshar, Amplified electrochemical sensor employing screen-printed electrode modified with Ni-ZIF-67 nanocomposite for high sensitive analysis of Sudan I in present bisphenol A, Food and Chemical Toxicology. 161 (2022). https://doi.org/10.1016/j.fct.2022.112824.

[41] D.N. Ta, H.K.D. Nguyen, B.X. Trinh, Q.T.N. Le, H.N. Ta, H.T. Nguyen, Preparation of nano-ZIF-8 in methanol with high yield, Canadian Journal of Chemical Engineering. 96 (2018) 1518–1531. https://doi.org/10.1002/cjce.23155.

[42] B. Manikandan, T. Endo, S. Kaneko, K.R. Murali, R. John, Properties of sol gel synthesized ZnO nanoparticles, Journal of Materials Science: Materials in Electronics. 29 (2018) 9474–9485. https://doi.org/10.1007/s10854-018-8981-8.

[43] V. Anh Tran, T. Khoa Phung, V. Thuan Le, T. Ky Vo, T. Tai Nguyen, T. Anh Nga Nguyen, D. Quoc Viet, V. Quang Hieu, T.T. Thi Vo, Solar-light-driven photocatalytic degradation of methyl orange dye over Co3O4-ZnO nanoparticles, Mater Lett. 284 (2021). https://doi.org/10.1016/j.matlet.2020.128902.

[44] G. Mohamed Reda, H. Fan, H. Tian, Room-temperature solid state synthesis of Co3O4/ZnO p–n heterostructure and its photocatalytic activity, Advanced Powder Technology. 28 (2017) 953–963. https://doi.org/10.1016/j.apt.2016.12.025.

[45] H. Wang, H. Wang, L. Li, Y. Gu, B.-H. Kim, J. Huang, Self-Powered Broadband Photodetectors Material Based on Co_3O_4–ZnO Heterojunction with Bottlebrush Nanostructure, ACS Appl Electron Mater. (2023). https://doi.org/10.1021/acsaelm.3c00311.

[46] Y. Sun, Z. Wang, W. Wang, G. Li, P. Li, K. Lian, W. Zhang, S. Zhuiykov, J. Hu, L. Chen, Electrospinning preparation of Pd@Co3O4-ZnO composite nanofibers and their highly enhanced VOC sensing properties, Mater Res Bull. 109 (2019) 255–264. https://doi.org/10.1016/j.materresbull.2018.10.001.

[47] S.Y. Alfaifi, W.A. Adeosun, A.M. Asiri, M.M. Rahman, Sensitive and Rapid Detection of Aspartic Acid with Co3O4-ZnO Nanorods Using Differential Pulse Voltammetry, Biosensors (Basel). 13 (2023). https://doi.org/10.3390/bios13010088.

[48] Y. Feng, Z. Li, C.Q. Cheng, W.J. Kang, J. Mao, G.R. Shen, J. Yang, C.K. Dong, H. Liu, X.W. Du, Strawberry-like Co3O4-Ag bifunctional catalyst for overall water splitting, Appl Catal B. 299 (2021). https://doi.org/10.1016/j.apcatb.2021.120658.

[49] E. López-Fernández, J. Gil-Rostra, C. Escudero, I.J. Villar-García, F. Yubero, A. de Lucas Consuegra, A.R. González-Elipe, Active sites and optimization of mixed copper-cobalt oxide anodes for anion exchange membrane water electrolysis, J Power Sources. 485 (2021). https://doi.org/10.1016/j.jpowsour.2020.229217.

[50] J. Sahu, P.A. Alvi, V.S. Vats, R.S. Meghwal, H. Sublania, D.M. Phase, M. Gupta, S. Kumar, S. Dalela, Annealing Temperature Dependence of Various Properties of ZnO Nanoparticles Investigated with Soft XAS, Nano. 16 (2021). https://doi.org/10.1142/S1793292021501307.

[51] A. Sharma, M. Varshney, H.J. Shin, B.H. Lee, K.H. Chae, S.O. Won, Effect of Cu insertion on structural, local electronic/atomic structure and photocatalyst properties of TiO2, ZnO and Ni(OH)2 nanostructures: XANES-EXAFS study, Mater Chem Phys. 191 (2017) 129–144. https://doi.org/10.1016/j.matchemphys.2017.01.008.

[52] R. Zhang, L. Pan, B. Guo, Z.F. Huang, Z. Chen, L. Wang, X. Zhang, Z. Guo, W. Xu, K.P. Loh, J.J. Zou, Tracking the Role of Defect Types in Co3O4 Structural Evolution and Active Motifs during Oxygen Evolution Reaction, J Am Chem Soc. 145 (2023) 2271–2281. https://doi.org/10.1021/jacs.2c10515.

[53] S. Samanta, P. Srinivasan, J.B.B. Rayappan, K. Kailasam, Ru quantum dots decorated graphitic carbon nitride (Ru-QDs@g-CN) for chemi-resistive sensing of 3-methyl-1-butanol at room temperature, Sens Actuators B Chem. 368 (2022). https://doi.org/10.1016/j.snb.2022.132060.

Supporting information

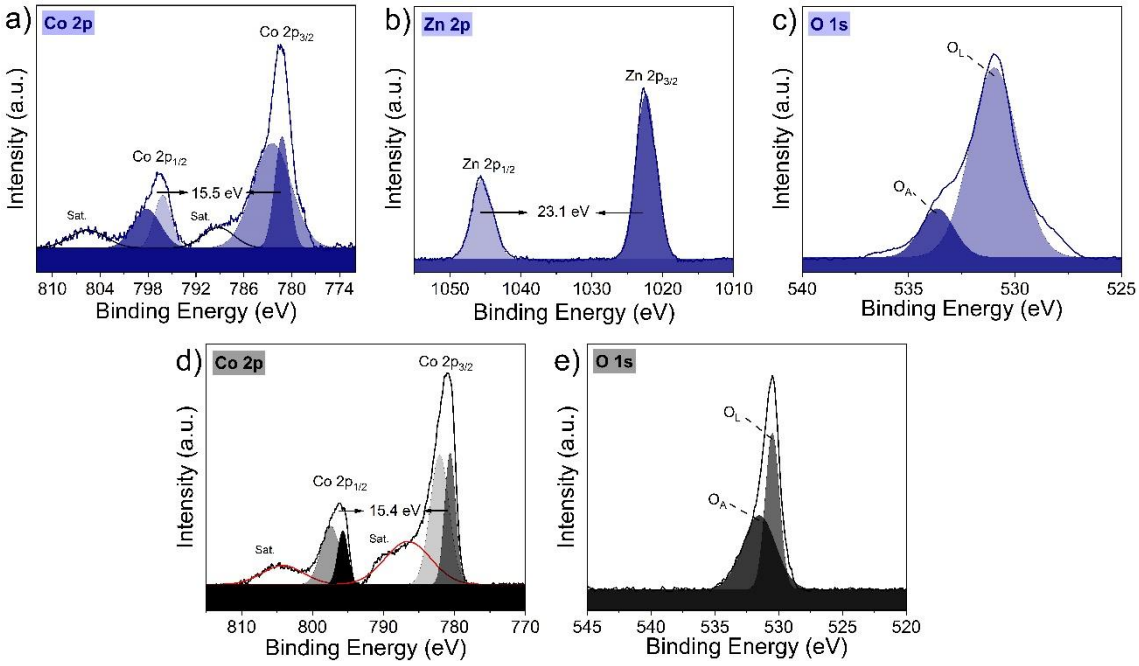

Fig. S1. High-resolution XPS spectra from (a) Co 2p, (b) Zn 2p, and (c) O 1s of the ZnO-Co_3O_4, and (d) Co 2p and (e) O 1s of the Co_3O_4.

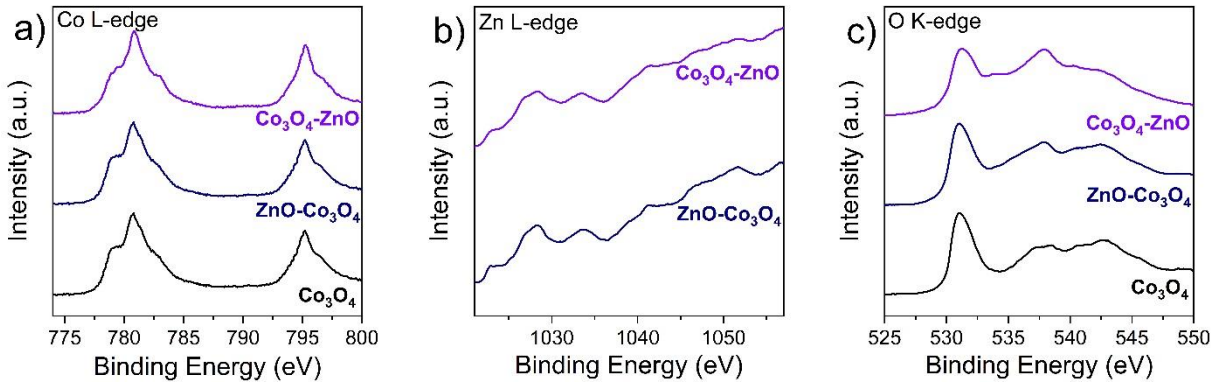

Fig. S2. XAS spectra in TFY around the (a) Co, (b) Zn, and (c) O K-edges of the Co_3O_4, ZnO-Co_3O_4, and Co_3O_4-ZnO.

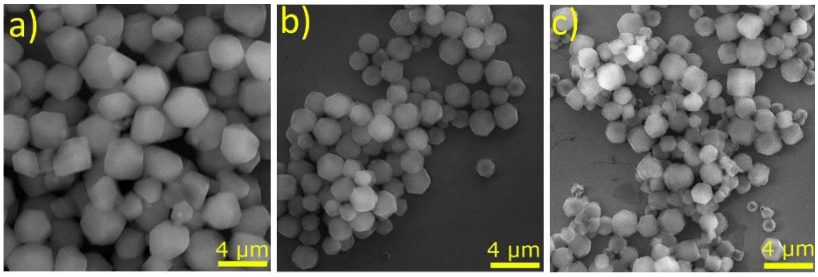

Fig. S3. FESEM images of (a) ZIF-67, (b) ZIF-8-ZIF-67, and (c) ZIF-67-ZIF-8

CHAPTER 4: Conclusions and future challenges

The present study explored the potential of a heterostructured material suitable for MVOC detection at different operation conditions. As discussed in Chapter 2, MVOCs cause several problems related to human health, especially the presence of pathogens composed of fungi and bacteria. In this way, MVOC detection with high selectivity and low cost contributes to mitigating these social situations, creating a database of MVOCs. The synthesized Co_3O_4-ZnO exhibited an excellent sensing performance, especially for 3-methyl-1-butanol detection, with a simple synthesis method (Chapter 3). Besides, this *p-n* heterostructure presented a higher response for 3M1B at the optimal temperature, lower response time, and higher selectivity ratio between all the synthesized sensors (Co_3O_4 and ZnO-Co_3O_4).

The upcoming challenges are summarized in a better characterization of the synthesized Co_3O_4-ZnO, such as Transmission Electron Microscopy (TEM) and band-gap energy value measurement. These techniques can bring more information about the material and understand the electronic changes caused by the *p-n* heterojunction. The sensing performance for 3M1B, as discussed in Chapter 3, can be better explained by the mechanism occurring at the surface of the material and band-gap study. Moreover, it is essential to study the selectivity measurements with MVOCs produced by a specific bacterium, such as the compounds liberated by the *Pseudomonas spp* discussed in Chapter 2 (3-methyl-1-butanol, 2,4-dimethyl-1-heptane and 2-butanone).

Finally, this study can assist other people in the group who pretend to work with *p-n* heterostructures, MOFs as precursors for SMO synthesis, ZnO and Co_3O_4 characterizations, and 3M1B detection. The increase in MVOCs database is an exciting aim of the group. So, with more information about these compounds and how one can influence a selectivity factor, more knowledge and growing up with the use of sensors. Besides, measurements with conditions close to real, such as temperature and relative humidity, are also challenging to overcome.

References

ARAÚJO, E. A. et al. Synthesis, growth mechanism, optical properties and catalytic activity of ZnO microcrystals obtained via hydrothermal processing. **RSC Advances**, v. 7, n. 39, p. 24263–24281, 2017.

BAHOS, F. A. et al. ZIF nanocrystal-based surface acousticwave (SAW) electronic nose to detect diabetes in human breath. **Biosensors**, v. 9, n. 1, 1 mar. 2019.

BOS, L. D. J.; STERK, P. J.; SCHULTZ, M. J. **Volatile Metabolites of Pathogens: A Systematic Review**. **PLoS Pathogens**, maio 2013.

CHOOPUN, S.; HONGSITH, N.; WONGRAT, E. Metal-Oxide Nanowires for Gas Sensors. Em: **Nanowires - Recent Advances**. [s.l.] InTech, 2012.

DJURIŠIĆ, A. B.; LEUNG, Y. H.; CHING NG, A. M. **Strategies for improving the efficiency of semiconductor metal oxide photocatalysis**. **Materials Horizons**Royal Society of Chemistry, , 1 jul. 2014.

FAN, Y.; SCHNEIDER, K. R.; SARNOSKI, P. J. Determining spoilage of whiteleg shrimp (Litopanaeus vannemei) during refrigerated storage using colorimetric strips. **Food Chemistry: X**, v. 14, 30 jun. 2022a.
FAN, Y.; SCHNEIDER, K. R.; SARNOSKI, P. J. Determining spoilage of whiteleg shrimp (Litopanaeus vannemei) during refrigerated storage using colorimetric strips. **Food Chemistry: X**, v. 14, 30 jun. 2022b.

GAI, L. Y. et al. **Recent advances in ethanol gas sensors based on metal oxide semiconductor heterojunctions**. **Rare Metals**University of Science and Technology Beijing, , 1 jun. 2022.

KHOT, L. R.; PANIGRAHI, S.; LIN, D. Development and evaluation of piezoelectric-polymer thin film sensors for low concentration detection of volatile organic compounds related to food safety applications. **Sensors and Actuators, B: Chemical**, v. 153, n. 1, p. 1–10, 31 mar. 2011.

KIM, H. J.; LEE, J. H. **Highly sensitive and selective gas sensors using p-type oxide semiconductors: Overview**. **Sensors and Actuators, B: Chemical**, 1 mar. 2014.

KIM, I. D.; ROTHSCHILD, A.; TULLER, H. L. Advances and new directions in gas-sensing devices. **Acta Materialia**, v. 61, n. 3, p. 974–1000, fev. 2013.

KISHORE KUMAR, D. et al. **Functionalized metal oxide nanoparticles for efficient dye-sensitized solar cells (DSSCs): A review**. **Materials Science for Energy Technologies**KeAi Communications Co., , 1 jan. 2020.

KORPI, A.; JÄRNBERG, J.; PASANEN, A. L. **Microbial volatile organic compounds**. **Critical Reviews in Toxicology**, fev. 2009.

KRISHNA, K. G. et al. **Nanostructured metal oxide semiconductor-based gas sensors: A comprehensive review**. **Sensors and Actuators A: Physical**Elsevier B.V., ,1 jul. 2022.

LI, P. Z.; ARANISHI, K.; XU, Q. ZIF-8 immobilized nickel nanoparticles: Highly effective catalysts for hydrogen generation from hydrolysis of ammonia borane. **Chemical Communications**, v. 48, n. 26, p. 3173–3175, 29 fev. 2012.

LÜ, Y. et al. MOF-Templated Synthesis of Porous Co $_3$ O $_4$ Concave Nanocubes with High Specific Surface Area and Their Gas Sensing Properties. **ACS Applied Materials & Interfaces**, v. 6, n. 6, p. 4186–4195, 26 mar. 2014.

MENG, D. et al. Low-temperature formaldehyde gas sensors based on NiO-SnO2 heterojunction microflowers assembled by thin porous nanosheets. **Sensors and Actuators, B: Chemical**, v. 273, p. 418–428, 10 nov. 2018.

MOKOENA, T. P.; SWART, H. C.; MOTAUNG, D. E. A review on recent progress of p-type nickel oxide based gas sensors: Future perspectives. **Journal of Alloys and Compounds**, v. 805, p. 267–294, 15 out. 2019.

SANTOS-CARBALLAL, D. et al. Al2O3/ZnO composite-based sensors for battery safety applications: An experimental and theoretical investigation. **Nano Energy**, v. 109, 1 maio 2023.
SHU, Y. et al. Ni and NiO Nanoparticles Decorated Metal-Organic Framework Nanosheets: Facile Synthesis and High-Performance Nonenzymatic Glucose Detection in Human Serum. **ACS Applied Materials and Interfaces**, v. 9, n. 27, p. 22342–22349, 12 jul. 2017.

THORN, R. M. S.; GREENMAN, J. **Microbial volatile compounds in health and disease conditions**. **Journal of Breath Research**, jun. 2012.

TURGUT, E. et al. Oxygen partial pressure effects on the RF sputtered p-type NiO hydrogen gas sensors. **Applied Surface Science**, v. 435, p. 880–885, 30 mar. 2018.

WANG, C. N. et al. Advances in Doped ZnO Nanostructures for Gas Sensor. **Chemical Record**, v. 20, n. 12, p. 1553–1567, 1 dez. 2020.

WANG, Y. et al. **Microbial volatile organic compounds and their application in microorganism identification in foodstuff**. **TrAC - Trends in Analytical Chemistry**Elsevier B.V., , 1 abr. 2016.

WEISSKOPF, L.; SCHULZ, S.; GARBEVA, P. **Microbial volatile organic compounds in intra-kingdom and inter-kingdom interactions**. **Nature Reviews Microbiology**Nature Research, , 1 jun. 2021.

XU, J.; LIU, S.; LIU, Y. Co3O4/ZnO nanoheterostructure derived from core-shell ZIF-8@ZIF-67 for supercapacitors. **RSC Advances**, v. 6, n. 57, p. 52137–52142, 2016.

YAN, W. et al. MOF-Derived Porous Hollow Co3O4@ZnO Cages for High-Performance MEMS Trimethylamine Sensors. **ACS Sensors**, v. 6, n. 7, p. 2613–2621, 23 jul. 2021.

YAN, Y. et al. Facile synthesis of an accordion-like Ni-MOF superstructure for high-performance flexible supercapacitors. **Journal of Materials Chemistry A**, v. 4, n. 48, p. 19078–19085, 2016.

YUAN, H. et al. **Metal-Organic Framework Based Gas Sensors**. **Advanced Science**John Wiley and Sons Inc, , 1 fev. 2022.

ZAKI, S. E. et al. Role of oxygen vacancies in vanadium oxide and oxygen functional groups in graphene oxide for room temperature CO2 gas sensors. **Sensors and Actuators, A: Physical**, v. 294, p. 17–24, 1 ago. 2019.